SUBSIDENCE DETERMINATION BY AERIAL PHOTOGRAMMETRY

C. ARMENAKIS

May 1983

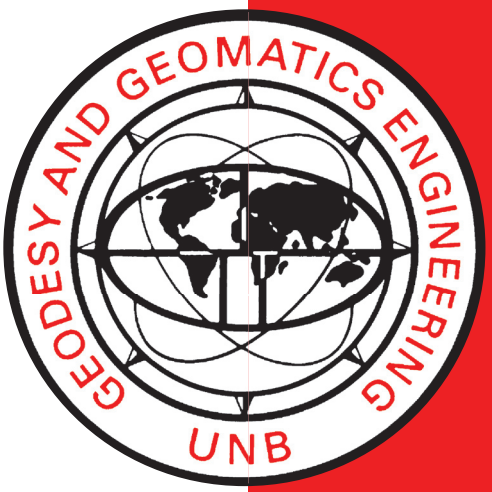

TECHNICAL REPORT
NO. 93

PREFACE

In order to make our extensive series of technical reports more readily available, we have scanned the old master copies and produced electronic versions in Portable Document Format. The quality of the images varies depending on the quality of the originals. The images have not been converted to searchable text.

SUBSIDENCE DETERMINATION BY AERIAL PHOTOGRAMMETRY

Costas Armenakis

Department of Surveying Engineering
University of New Brunswick
P.O. Box 4400
Fredericton, N.B.
Canada
E3B 5A3

May 1983
Reprinted December 1987

PREFACE

This report is an unaltered version of the author's M.Sc.E. thesis submitted to this Department under the same title.

The financial support of the National Science and Engineering Research Council is thankfully acknowledged as well as the cooperation of CANMET, Calgary, B.C. Coal, Sparwood, and Ecological and Resources Consultants, Fredericton, who provided most of the data for this study.

The advisor of this work was Dr. Wolfgang Faig, whose assistance is highly appreciated.

The assistance lent by others is given in detail in the acknowledgements of the author's M.Sc.E. thesis.

ABSTRACT

The demand for extensive exploitation of natural resources has led to an increase in underground mining activities. After the extraction of material the overlying strata settle to fill the empty spaces causing cavings and crevices. Consequently, subsidence may occur on the ground surface. The effects of surface ground subsidence have caused serious problems to society, including the loss of human lives, extensive property damage, disruption of communications, as well as environmental concerns.

Monitoring of subsidence can provide important information about both magnitude and trends. Therefore, effective preventive methods must be developed to control the subsidence phenomena. Among other surface monitoring methods, photogrammetry offers a useful tool for accurate monitoring of mining subsidence.

In this thesis, the causes of subsidence, as well as some interrelated factors influencing the amount and rate at which subsidence occurs, are presented. An overview of the various monitoring methods - physical and geometrical - is also given. The examination of the advantages and limitations of the different approaches shows why, when and how photogrammetry can play a major role in a monitoring system.

Depending on the purpose and accuracy of monitoring, four photogrammetric techniques are investigated in this study, which focusses on their applicability in highly mountainous terrain. These include comparison of contour lines, determination of displacements by

mathematically defined object points, determination of displacements by natural points and actual ground displacements from model coordinate differences.

The identification of discrete natural points is based on a 'cross-identification' procedure where the advantages of stereo-vision are fully utilized. Even though the first method is purely analogue, an error analysis of the uncertainty of the contour lines gives an indication of where it can be applied. Digital elevation model techniques and the application programs of the analytical plotter AP-2C (O.M.I.) are combined to study subsidence of mathematically defined object points. Problems encountered on steep slopes are examined. In the third technique, the performance of two bundle adjustment programs with self-calibration are studied, while the displacements are computed as coordinate differences between two epochs. Due to extreme topographical conditions of the mining site, surveying and resurveying of control - and check points is quite problematic. The need to know the displacements with respect to the same reference datum led the author to develop a fourth photogrammetric technique, presented in this thesis. Displacements are determined in the model space and then transferred to the ground via four elements of the absolute orientation of one epoch only.

Finally, an example of a study area is given, with statistical tests applied to evaluate the usefulness of the photogrammetric monitoring system.

TABLE OF CONTENTS

TABLE OF CONTENTS (Cont'd)

LIST OF TABLES

LIST OF FIGURES

NOTATIONS

A	:	first design matrix
$\bar{A}_i$, $\bar{A}_j$	:	rays connecting the camera stations with a model point
$\bar{a}_i$, $\bar{a}_j$	:	rays connecting the camera stations with a photo point
α	:	significance level
b	:	photographic base
$\bar{B}$	:	model base
$\bar{B}_x$, $\bar{B}_y$, $\bar{B}_z$	:	components of the model base
B	:	second design matrix
$C_{\Delta\hat{x}_{ij},\Delta\hat{y}_{ij},\Delta\hat{z}_{ij}}$	:	variance-covariance matrix of the components of displacements
$C_{\Delta S_p}$	:	variance-covariance matrix of the sample
c	:	value of a quadratic form
Δp	:	change in stereoscopic x-parallax
Δh	:	change in ground elevation
$\Delta\Theta$	:	atmospheric refraction
$\Delta S_{p_{ij}}$	:	displacement vector
Δr	:	radial lens distortion correction
ΔR	:	atmospheric refraction correction
dX, dY	:	horizontal coordinate changes of a point on the projection plane
d	:	scalar multiplier

db_x, db_y, db_z	:	changes of the model base of a photogrammetric instrument
$d\omega$, $d\phi$, $d\kappa$	:	changes of the orientation of a projection of a photogrammetric instrument
df	:	degrees of freedom
dX_M, dY_M, dZ_M	:	components of model displacement vector
DX, DY, DZ	:	components of ground displacement vector
$\bar{e}$	:	vector of minimum distance between two conjugate rays
$E(r_n)$	:	expectation value of r_n's
ζ	:	statistic value of a quadratic form
f	:	focal length
F, F_1, F_2, F_3	:	expanded functional forms
H	:	flight altitude
H'	:	average height
h	:	ground elevation
H_Z	:	number of horizontal control points
H_o	:	null hypothesis
L	:	observation vector
λ	:	scale factor
λ_1, λ_2	:	scalar multipliers
M_j	:	rotation matrix
m_{ij}	:	elements of the rotation matrix
μ_r	:	mean value of r_n's
$\xi_{\chi^2_{u,1-\alpha}}$	:	critical value of the x^2-distribution

p	:	stereoscopic x-parallax
P	:	weight matrix
Q	:	variance-covariance matrix of the unknown parameters.
r	:	radial distance between a photo-point and its principle point
r_p	:	residual parallaxes
$\bar{r}$	:	photo-residuals
r_n	:	difference between photogrammetric and surveying results
$R_{(\Omega,\Phi,K)}$	:	rotation matrix
r_{ij}	:	elements of the rotation matrix R
s	:	scale factor
$\hat{\sigma}_o^2$	:	a-posteriori variance factor
$\sigma_{\Delta s}^2$	:	variance of the displacement vector Δs
Σ	:	variance-covariance matrix of the population
$\Sigma_{\hat{x}_i}$	:	variance-covariance matrix of the computed ground points
u_i, v_i, w_i	:	rotated photo-coordinates of the left photograph
V	:	vector of residuals
V_R	:	number of vertical control points
W	:	misclosure vector
$X_{M_i}, Y_{M_i}, Z_{M_i}$	:	model coordinates

$X_{i_G}, Y_{i_G}, Z_{i_G}$	:	ground coordinates
X_T, Y_T, Z_T	:	translation vectors
X_{OM}, Y_{OM}, Z_{OM}	:	translation vectors
$\hat{X}$	:	least squares estimate
X_i^c, Y_i^c, Z_i^c	:	coordinates of the camera station
x, y	:	refined photo-coordinates
x_o, y_o	:	coordinates of the principle point
χ^2	:	chi-square distribution
$\omega_j'', \phi_j'', \kappa_j''$	:	orientation of the right photograph with respect to the left one

1

INTRODUCTION AND PREVIOUS STUDIES

Deformations can occur in structures such as buildings and dams, as well as in the uppermost layer of the earth's crust due to ground compression. These types of deformations manifest themselves predominantly as a local or regional* subsidence. Surface subsidence may be caused by extraction of underground water, oil and gas *(Vanicek et al., 1982)*. Mining conditions, combined with a particular geological structure of overlying strata, can also lead to the subsidence phenomena (Chapter 2, section 2.3).

The effects of the extraction on the ground surface may range from cavings and crevices to land settlement and creation of gentle subsidence basins, depending on the depth of the exploitation and on the rock-mechanic parameters of the soil.

The necessity for monitoring the ground deformations is dictated by the extensive damage they cause. Across the United States alone, damage due to mining subsidence has already affected over 8 000 km^2 of land of which about 600 km^2 are in urban areas

* Definitions are given in Appendix IV.

(Chrzanowski et al., 1983). During the next 20 years 6 000 to 10 000 km^2 will be affected by underground mining. Unless effective preventive methods can be developed to control subsidence, damage may be caused at an estimated cost of at least $2 billion (U.S.) *(ibid.)*.

Despite several existing theories (deterministic or statistical) of subsidence *(Chrzanowski, 1979)*, which give a good agreement between the predicted and the practical values for specific mining conditions, there is no one general theory which can be successfully applied to any mining and geological conditions *(Chrzanowski et al., 1980)*. The objective of this study is to examine the applicability of aerial photogrammetry as a surface monitoring method in highly mountainous terrain. This approach provides 3-dimensional information about external deformations, with sufficient accuracies, in difficult mining and topographical conditions. The photogrammetric results, beyond their practical interest, can also contribute to the improvement of the prediction theories through the gaining of more knowledge about the behavior of the rock masses.

A review of the literature, which follows, shows that photogrammetric techniques have been used as monitoring methods. There are essentially two approaches to measuring displacements. First, the spatial coordinates of the points are determined directly and then the coordinate differences between the time lapse give the vectors of displacements. Secondly, movements in one plane can be determined using the time-parallax method.

Faig *(1965)* has used aerial photographs to determine horizontal movements of a glacier along a certain profile. A motion parallax method has been studied with reduced parallax values due to

tilt and flying height. It neglects differences of second order such that accuracy is mainly affected by the chosen flying height *(Konecny, 1963)*. Borchers *(1968)* has given examples of terrestrial photogrammetry for monitoring structural deformations. Analytical terrestrial photogrammetry also has been applied to determine deformations of targetted points on a dam structure *(Brandenberger et al., 1972)*.

Measurements of surface subsidence over mines and excavated salt domes have been presented by Brown *(1973)*. Targets over the area were triangulated from a set of 16 microflat plates of scale about 1/9000 with DBA plate camera. In this case, analytical triangulation produced accuracies competitive with those of first-order ground surveying. Relative to the major dimension of the area, the RMS difference between photogrammetric and exhaustive first-order ground surveys were found to amount to 1/238000 horizontally and 1/150000 vertically *(Brown, 1981)*. Since convergent photography was used, this design is not appropriate for map compilation.

The practical and economical potential of analytical photogrammetry with terrestrial cameras has been applied to the monitoring of structural deformations *(Erlandson, 1975)*. Simulated results of a sensitivity analysis of a photogrammetric network have been given by Fraser *(1982)*. Peterson *(1976)* presented the use of photogrammetry in detecting the displacements of structures or slide areas. Terrestrial and aerial photogrammetric methods were used. The latter was a large departure from the former since two potential problems were introduced which were not encountered before. First, the photograph was on film instead of on glass plates, and hence subject to differential shrinkage. Secondly, the camera locations and orientation angles were no longer

known so these quantities had to be determined by a space resection. However, even though an improved version of the standard resection solution was adapted, it is noted that the photogrammetric system should be used with caution until more extensive data can be collected concerning its applicability.

Improvement in the accuracy of monitoring can be obtained with a combination of aerial and terrestrial convergent photographs *(Veress et al., 1981)*. This method would free the photogrammetric application from restrictions *(Veress, 1982b)*, thus allowing the practitioner to obtain the optimum geometry for the monitoring system even when the terrain features do not permit favorable location of the terrestrial camera platform or when the complete structure cannot be imaged on aerial photographs. However, difficulties may arise in mountainous terrain with dense vegetation coverage when non-targetted points are used, in addition to the mapping requirements.

In underground mining, photogrammetry has been used to investigate displacements of the walls and roofs of the tunnels. Dauphin et al. *(1977)* have used single photographs since displacements on a vertical plane were only required. To circumvent the point identification over long time lapses, the same authors used a modified time-parallax procedure. Mine roof instability has also been studied through rock face deformation and slope stability *(Allam, 1976; Bradow et al., 1976; Derenyi, 1972; Robertson et al., 1982)*. In a related application the determination of temporal deformations of a retaining wall was done by terrestrial photogrammetry *(Veress et al., 1978; 1980)*. Pre-marked points were measured while

the scale was approximately 1/1640. The photographic distance was about 1 000 m and a modified aerial camera with focal length of 610 mm was employed to satisfy the required accuracies. Ordinary aerial photographs of scales 1/18000 and 1/24000 have been used to detect displacements of sliding areas *(Kölbl et al., 1982)*. The displacements were rather large (≈ 0.5-19 m) and the achieved accuracy depending on the photo scale was 20 to 40 cm.

Veress *(1982a)* presented another case of monitoring an ancient slide area through the use of aerial photographs. Targets were bolted to suitable rocks, distributed over the area. A comparison analysis on the discrepancies between photogrammetric and surveying data at control points led to an average relative accuracy of about 1/45000.

Recently, the applications of digital terrain and digital elevation models in the mining industry have provided satisfactory results for monitoring volume changes *(Johnson et al., 1982; Fenton, 1982; Toomey, 1982)*. Thus ground subsidence can also be determined as vertical differences of digital elevation models representing the area of interest in two different epochs of time *(Somogyi, 1982)*.

Furthermore, for identifying subsidence problem areas, the application of aerial remote sensing techniques have been examined in considerable detail in an attempt to determine more efficient and cost-effective means *(Earth Satellite Corporation, 1975)*. The features used to derive subsidence data from aerial imagery are landforms, tones, vegetation patterns, photographic textures, and photographic lineations *(Norman et al., 1975)*.

Landsat and SLAR imageries are used to detect fractures, regional lineaments and fault patterns, as well as to trace unstable mine roofs *(Sullivan, 1978)*. Aerial photos were used to detect regional subsidence, fracture traces pothole subsidence and linear subsidence *(Russel et al., 1979)*.

In addition to the present photogrammetric and remote sensing techniques, a telemetric system for monitoring relative displacements of ground subsidence in mining areas has been developed and successfully tested under very difficult topographic and climatological conditions *(Chrzanowski et al., 1982c; Fisekci et al., 1981)*. The system was based on an array of tiltmeters with a sophisticated microprocessor-based radio transmittance of the tilt signals to a computer controlled central station *(Chrzanowski et al., 1982b)*.

So far, in almost all the applications of aerial photography, targetted points were used for monitoring quite smooth terrains. However, since some subsidence phenomena are unpredictable and may occur in areas not covered by targets, practical disadvantages are encountered. Also, the installation and maintenance of targets in highly mountainous terrain is not always practicable. Therefore, the use of non-targetted points was investigated as an alternative with respect to different photogrammetric techniques.

Difficulties in resurveying ground control points before each new flight due to extreme topographical conditions led to the development of the direct determination of actual object displacements from model coordinate differences. At the present time, even though bundle adjustment programs with self-calibration are available,

convergent photography was impossible because vertical photography was flown such that is could also be used for mapping.

In Chapter 2 the land surface subsidence problems caused by underground mining is presented. The geological and mining conditions which cause subsidence are explained, as well as the necessity of monitoring the ground deformations. Furthermore, an analysis of the monitoring methods is given with their advantages and limitations. In this context, photogrammetry is investigated as a part of an integrated monitoring system.

A detailed study of the photogrammetric techniques for monitoring surface subsidence was carried out by the author and is given in Chapter 3. Beginning with the comparison of contour lines and their error-analysis, we then proceed to the determination of movements along profiles and in digital elevation models. The various differences in using these two methods over flat and mountainous terrain and the problems encountered are discussed. Natural points, selected by cross-identification are then used to determine displacements. Two approaches were studied: First, the absolute ground coordinates provide information about the displacements between the time lapse. Secondly, a method is proposed whereby ground control points are necessary only in one of the different epochs. This epoch is called the zero epoch. The photogrammetric models* of the area are formed for the zero and the t_1 epoch, respectively. The photogrammetric model formation is done analytically utilizing the proper mathematical model and the measured coordinates of photo-points.

---

* Definitions are given in Appendix IV.

Subsequently, the model of the zero epoch is absolute oriented*. Ground coordinates of the measured photo-points are computed and four of the seven absolute orientation parameters (scale and three rotations) are stored. Then the model of epoch t_1 is transferred to the model coordinate system of the zero epoch. The transformation is performed with the aid of reference points. These points lie out of the area influenced by subsidence, and usually are well recognized points in both epochs (corners of houses, poles, stones, etc.). At this stage, both epochs refer to a common datum. Points which have been affected by subsidence will have two sets of model coordinates with respect to the common system of the zero model. The model coordinate differences between the two epochs can then be transformed to ground displacements utilizing the already stored four transformation parameters. The mathematical model, as well as the description of the developed software are given for this approach.

The estimated accuracies of the photogrammetric techniques are presented in Chapter 4. One- and three-dimensional tests provide the accuracies of displacements derived photogrammetrically. The compatibility between surveying and photogrammetric results is also tested.

A test area for subsidence in mountainous terrain was used to study the four photogrammetric techniques. Chapter 5 contains a description of the area, numerical results and accuracies of the photogrammetric methods and a cost comparison between photogrammetry and ground surveying techniques.

---

* Definitions are given in Appendix IV.

A summary of the present study and the author's conclusion and recommendations are presented in Chapter 6.

2

LAND SURFACE SUBSIDENCE AND MONITORING

2.1 Definition

For the purpose of this study surface subsidence is defined as local, predominantly downward, vertical displacement with little or no horizontal movement component *(American Geological Institute, 1962; Norman et al., 1975)*. Mining activities disturb the equilibrium of the field of stresses in the rock masses. This may cause settling or collapse of overlying rock formations as is shown in Figure 2.1 (section 2.3).

The subsidence effects are caving or distortion of the land surface, which in highly mountainous terrain can cause sliding movements.

2.2 The Problem of Mining Subsidence

Subsidence of the land surface may occur in many places at the mining areas. Surface subsidence in areas of underground mining has created serious hazards and caused extensive property damage in

many localities. According to Allana M. Sullivan *(1978)* "the number one killer in underground coal mines has been identified as roof fall." Mining is considered to present a subsidence hazard when the overburden weight exceeds the safe wall and roof strength.

Evidence of sinking is apparent at mining sites in the form of faults, cracks, fractures and in cracked or bent walls and foundations of buildings, broken piers and bridge abutments, uneven highway and rail beds, and the short steep grade of streets at railroad crossing. Subsidence has also caused ruptures in underground utility lines. Several instances have been reported where motor vehicles have sunk into cavities which opened up in streets, roads and highways; houses and other buildings have collapsed or have been tilted by caving under their foundations *(Russel et al., 1979)*. The damages due to subsidence are definitely a continuing problem.

The subsidence problem has been neglected here in Canada due to the remote location of many exploitation areas, without causing too many problems. Only relatively few mountain slides have occured, with the most serious being one near Frank, B.C., in 1903, where a village was buried!

2.3 Cause of Mining Subsidence

The relation between surface subsidence and underground mining operations is important since mining subsidence is caused basically by sub-surface mining works. Some of the major geological and mining conditions that are related to underground mine roof failures, which might ultimately result in surface subsidence, are shown in Figure 2.1.

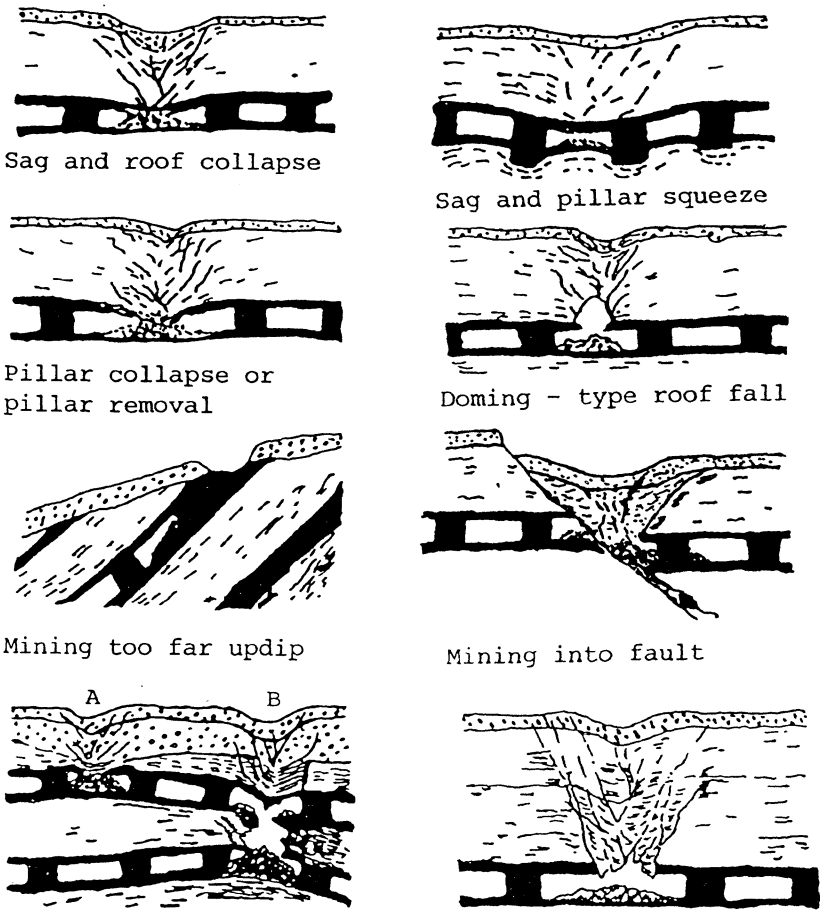

Figure 2.1: Surface subsidence due to geological and mining conditions.

During underground mining activities, the overlying strata has a tendency to cave in and, in most cases, will cave eventually to fill the void unless the working has been completely backfilled. Subsidence may eventually take place at the surface of the ground after sub-surface cavities occur. Many interrelated factors influence the amount of surface subsidence and the rate at which subsidence

occurs in a specific locale.

Geological structure of the area, strength of rock materials and mining techniques are included in these factors. More specifically, these components are the intensity and depth of mining, the thickness and number of coal beds mined, the composition, thickness, and degree of consolidation of the overlying strata, the type and amount of roof support for the mining operations, and structural features such as the steepness of the dip angle of the coal seam and the presence of planes of weakness (i.e., inclined bedding planes, joints and faults). Each example of subsidence is almost unique because the factors mentioned do not affect individually, but may be combined in various ways. Figure 22 illustrates a diagram of these factors.

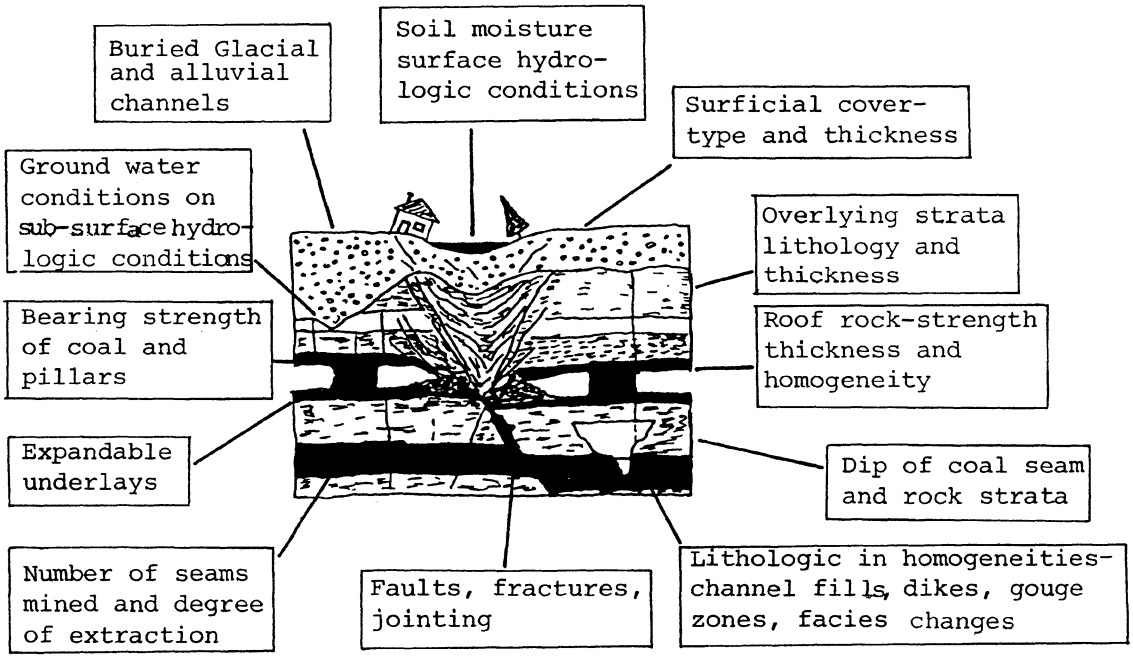

Figure 2.2: Geological factors resulting surface subsidence.

2.4 The Necessity of Monitoring Surface Subsidence

Subsidence monitoring is to be considered in conjunction with extensive analysis and interpretation of the geometric subsidence deformation values. The analysis will provide metric information about both the measurements and the deformable body. Statistical tests concerning the accuracy of the computed displacements, recording of the interrelated activities between underground mining workings and surface subsidence, and rate of movements with respect to time are some typical examples of analysing deformations. The main goal of the interpretation is to define the relationship between causative effects (loading forces) and responsive effects (deformations).

The observed deformations can be studied either with respect to the deformable body or by deriving information about the load-deformation relationship *(Chen et al., 1982)*. In the first case, the final results will provide information about relative displacements of discrete points of the entire body. In the second case, the additional knowledge about the load-deformation relationship is obtained by using either a deterministic or a stochastic (empirical method *(ibid.)*.

A more meaningful comparison between the designed and observed deformations is allowed through deterministic modelling of the relationship among causative effects, material properties, and deformations. This type of modelling is performed by sophisticated numerical procedures, such as the finite element method. On the other hand, the stochastic method models the load-deformation relationship by analysing the correlation between the responsive results with the causative effects *(Chrzanowski et al., 1983)*. This correlation allows a comparison with the design model which in turn

leads to adjustment (improvement) of the latter.

Consequently, the analysis and interpretation of deformation measurements become very important and complex. Therefore, strong cooperation between the surveying engineer and specialists in geotechnical, geophysical, rock mechanics and related fields is necessary during the entire life of the project. A better design of a mining project will i) improve safety conditions to prevent or reduce danger to human lives, ii) reduce the loss of capital cost caused by extensive property damage and disruption of operations or general communications, and iii) be a study-example for future designs.

2.5 Methods of Monitoring Subsidence-Advantages and Limitations

It is necessary to determine the magnitude and the direction of motions of subsidence areas in order to obtain an insight into their character either for reasons of safety or for future design criteria. Present methods for detecting and monitoring subsidence can be divided into two basic groups; physical and geometric *(Chrzanowski, 1981)*.

Physical methods are used to measure relative displacements by various mechanical instruments such as tiltmeters, extensometers, inclinometers, strain gauges, feeler gauges, rock noise listening devices, etc. Although the precision of measurement by means of these instruments may be high, the results only yield information about the displacement of one point in the body with respect to another. That is, the information about the displacement of any one separate point in incomplete. Therefore, the physical monitoring systems

must be associated with geometric methods. Geometric methods measure absolute displacements, ie., displacements of points with respect to some stable reference. These are geodetic and photogrammetric methods.

Although geodetic methods can provide higher absolute accuracies, they are based solely on data obtained at specific points. Thus the system is point dependent. The time needed for a comprehensive survey may often cover several stages. This means that actual movements may be left undetected and may thus reduce the accuracy of the survey.

Photogrammetric methods are a surface monitoring system which basically eliminate some of the disadvantages of the classical field survey. The basic unit of the photogrammetric approaches is the photograph, aerial or terrestrial. A photograph represents a remote, complete and instantaneous record of an object, which in this case is the terrain affected by subsidence. An instantaneous record of a particular situation which may be changing in time, together with a complete coverage, is most suitable for an area phenomenon such as subsidence. The possibility of going back to a previous stage makes photography extremely useful for this purpose.

With the use of the cross-identification method, (Chapter 3), the photogrammetric approach does not require formal targets, except for a limited number of control points. In addition to the aforementioned, this provides many advantages when compared to geodetic measurement systems which require targets. Some of these advantages are:

-- The displacement of abrupt slopes which are inaccessible can be safely measured.

-- There is virtually no limit to the number of points which can be measured on the photographs with the implementation of natural points.

-- The detection of the early stages of slope failures over large areas, which could be difficult to be covered adequately by other methods.

-- It is a permanent record of observation, in the form of photographs. These photographs provide a historical record, which makes it possible to go back in time to establish a new naturally existing point near to one which has been lost and to re-establish the displacement history of the new point, or to re-examine the deformation history of an area in greater detail.

-- The cost of measuring a large number of points is lower.

-- All the points are measured simultaneously due to instantaneous property of the photographs.

-- The time required for storage of information is independent of the number of the measured points, and thus the field surveying time is reduced.

-- At little additional expense, wider coverage of the area can be achieved.

-- Photographs can be used for other purposes such as geological photointerpretation, volume determination, mapping requirements, digital elevation models, etc.

However, photogrammetric methods are also subject to some limitations:

-- Difficulties in precisely locating the same point on subsequent photographs, which is aggravated by surface deterioration of the soil and shadow combinations which change with time.
-- Occasional problems with surveying of the control points.
-- Accuracy of the ground control points.
-- Lapse of time until the evaluation of the data is done. The data conversion from photography to displacement results generally takes several days, which is not adequate for most active slope collapses.
-- Light and exposure differences.
-- Weather conditions at the area of interest.
-- The requirements of computer access, photogrammetric instruments and trained personnel (high capital cost).
-- Accuracy. Although the accuracies achieved are not so high as those from the geodetic method, they satisfy the design standards for many engineering applications.

No matter what method for the determination of displacements will be adapted, measurements must be carried out at least twice, each in a different epoch of time t_i.

2.6 Photogrammetry as a Monitoring System

In a modern design of an overall monitoring system, many disciplines and many different steps are involved. Engineers, geologists, photogrammetrists, surveyors, aerial photographers, and computer technicians must work together to achieve the

system goal; that is, to determine whether subsidence has occured over a period of time. In other words, the aim is the integration of surveying, rock mechanics, underground and photogrammetric methods for subsidence monitoring.

Before starting any monitoring method an insight into the problem is necessary. Quite often a combination of several methods, as already mentioned, will be required. If it is decided to employ photogrammetric methods, then the design must be made in such a manner as to obtain the strongest possible geometry according to available capacities and required accuracies. After the photographs have been taken the data analysis and processing follow. At this stage spatial displacements are calculated from photographic information and the results are evaluated and compared with any previous measurements, and, with any results obtained from any other method applied at the same area.

A difficult part of any monitoring process is the presentation of the results in concise form so that the engineer or other responsible person can evaluate the situation and make decisions. It is extremely useful that the final results be graphically illustrated, perhaps by computer plots. Figure 2.3 illustrates a diagram of the suggested steps for photogrammetric monitoring of surface subsidence.

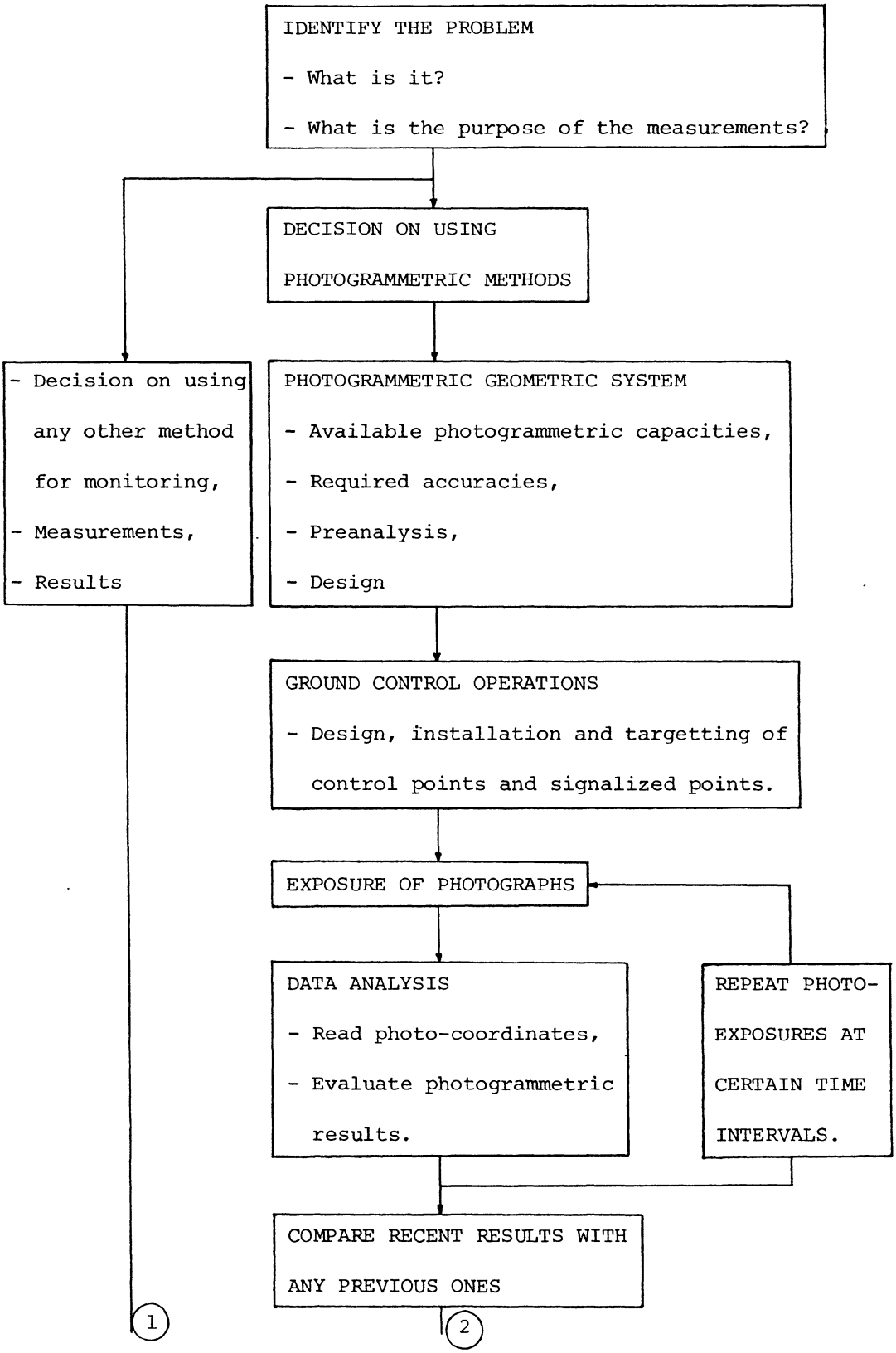
IDENTIFY THE PROBLEM
- What is it?
- What is the purpose of the measurements?
DECISION ON USING
PHOTOGRAMMETRIC METHODS
- Decision on using any other method for monitoring,
- Measurements,
- Results
PHOTOGRAMMETRIC GEOMETRIC SYSTEM
- Available photogrammetric capacities,
- Required accuracies,
- Preanalysis,
- Design
GROUND CONTROL OPERATIONS
- Design, installation and targetting of control points and signalized points.
EXPOSURE OF PHOTOGRAPHS
DATA ANALYSIS
- Read photo-coordinates,
- Evaluate photogrammetric results.
REPEAT PHOTO-EXPOSURES AT CERTAIN TIME INTERVALS.
COMPARE RECENT RESULTS WITH ANY PREVIOUS ONES
1
2

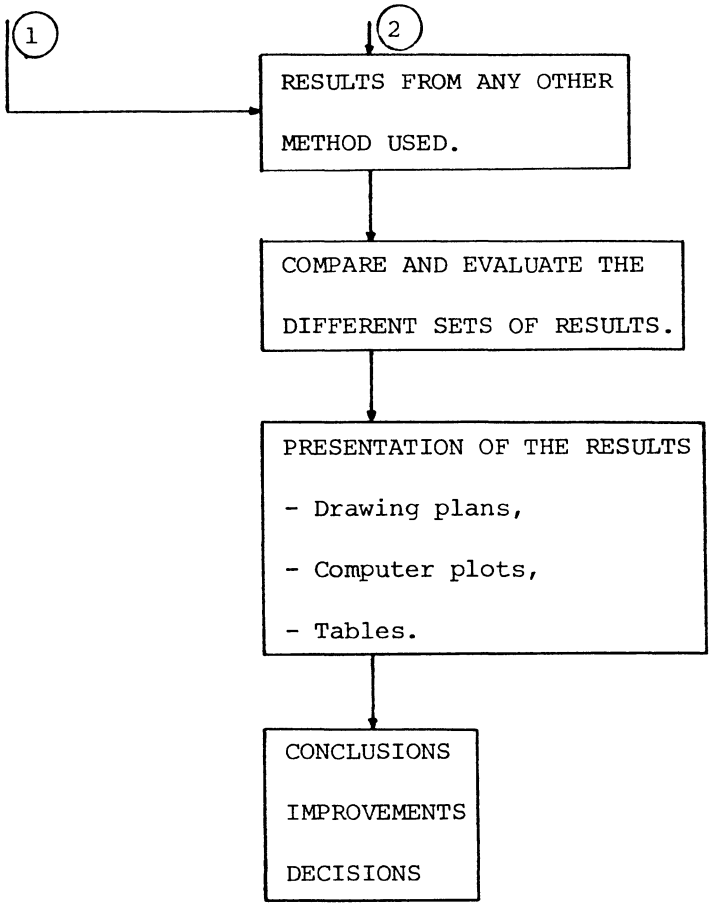

Figure 2.3: Flow diagram for monitoring surface subsidence by photogrammetry.

3

PHOTOGRAMMETRIC TECHNIQUES

Photogrammetry in land surface subsidence can be applied both qualitatively and quantitatively, provided that the area is covered at least twice, each at different epochs of time. Aerial and terrestrial photographs may be used for this purpose, as well as a combination of the two *(Veress et al., 1981)*.

The first aspect is purely interpretive where changes are detected, observed and recorded without further measurements *(Earth Satellite Corporation, 1975; Russel et al., 1973)*. Non-photographic sensors can be applied in a similar manner.

Actual movement values are determined by quantitative methods. There are basically four approaches:

-- Comparison of contour lines of the two epochs.

-- Movement determination using mathematically defined object points (i.e., grids, profiles).

-- Movement determination using physically defined object points (i.e., natural points).

-- Direct determination of object displacement vectors from model displacement vectors.

3.1 Contour Lines

3.1.1 Comparison of contour lines

Contour maps can be compiled for different epochs using the aerial photographs for each epoch. Contours can be plotted either on the same map sheet but with different colours or on different map sheets and then superimposed with the aid of reference points. Possible deformation of a point in horizontal and vertical position will be clearly visible from the graphical illustration *(Johnson, 1982)*.

However, the interpretation of the graphical plots presents two drawbacks. First, each contour line is characterized by a horizontal and vertical uncertainty. With a precision analogue plotter the internal accuracy is about 0.02 - 0.05% of the flying height *(Chrzanowski et al., 1982a)*. Secondly, possible sliding of the land surface will make the interpretation more difficult.

3.1.2 Vertical and horizontal uncertainty of the contour lines

The accuracy of terrain reproduction - getting metric information - from a map depends on the accuracy of the plotted contour lines. Consequently it is based on the accuracy of:

(i) The control points used for absolute orientation.

(ii) The photogrammetrical restitution to form the spatial model.

However the spatial model is never an exact replica of the photographed terrain due to several reasons, which can be divided into two groups *(Ghosh, 1972; Faig, 1976)*.

a) Non-orientation errors, due to:

- Residual photogrammetric refraction effects,
- Residual lens distortion effects,
- Film distortion and image plane deformation,
- Camera and instrument used,
- Operator's personal errors.

b) Orientation errors, due to:

- Interior orientation,
- Relative orientation,
- Absolute orientation.

The results of these errors may be interpreted in terms of x- and y-parallaxes. Thus, some of the corresponding pairs of rays may not intersect in space and some of those which intersect may not do so at the proper locations. However a part of model deformation can be compensated by the available elements of exterior orientation *(American Society of Photogrammetry, 1980)*.

(iii) Photo scale and plotting scale.

(iv) Contour interval.

Richardus *(1973)* has expressed the accuracy of contour lines in forms of variances using the concept of 'tubular confidence space' around the contour line, and Masry *(1977)* gives the variances of the point positions as functions of the errors in position (X^C, Y^C, Z^C) and attitude (ω, ϕ, κ) of the camera. Here the vertical and horizontal undertainty is interpreted in terms of x- and y-parallaxes.

3.1.2.1 Vertical uncertainty

The basic parallax equation, for a pair of true vertical photographs is given by *(American Society of Photogrammetry, 1980):*

$$p = \frac{fB}{H - h} \tag{3.1}$$

or

$$h = H - \frac{fB}{p} \tag{3.2}$$

where

h = elevation of a ground point

H = flight altitude

f = focal length

B = air base distance

p = stereoscopic x-parallax

It is to be noted that the derivation of this equation is based on

-- photographs without tilt

-- equal flight altitude

-- equal focal lengths.

While parallax eq. (3.1) serves to define stereoscopic parallax and its relationship to H,B, and f parallax differences are more convenient for determining elevations. It can be derived from eq. (3.1) for two points that:

$$\Delta h = \frac{\Delta p(H - h_1)}{p_1 + \Delta p} \tag{3.3}$$

$$\Delta p = \frac{p_1 \Delta h}{(H - h_1) - \Delta h} \tag{3.4}$$

in which

Δh = change in the value of h

h_1 = elevation of the lower of two points

p_1 = parallax of the lower point.

In stereoplotting instruments, parallax differences are not measured but are converted mechanically into elevation differences.

The major source of error in the computation of the elevations from using eq. (3.3) is the unavoidable presence of tilt. The presence of y-parallax is objectionable because it hinders stereoscopic vision. Film deformations caused by temperature and humidity variations introduce additional errors into the measurement. Also, observational errors represent another source of errors.

In practice, the average height (H') above the terrain is frequently used for the term $(H - h_1)$, and the average distance (photographic base b) between principal points and conjugate principal points is used for p_1. Thus, the simplified forms of eq. (3.3) and (3.4) are:

$$\Delta h = \frac{H'}{b + \Delta p} \Delta p \tag{3.5}$$

$$\Delta p = \frac{b}{H' - \Delta h} \Delta h \tag{3.6}$$

For cases where Δp is relatively small, the following approximations are sometimes useful *(American Society of Photogrammetry, 1980)*:

$$\Delta h = \frac{H'}{b} \Delta p \tag{3.7}$$

$$\Delta p = \frac{b}{H'} \Delta h \qquad (3.8)$$

The relative accuracy in determining elevations and drawing contours is indicated by eq. (3.7) and (3.1). The former equation shows that the differences in elevation is a factor times the parallax difference. Both terms in the factor are relatively strong: H' and b are usually known within, say, 2 percent *(American Society of Photogrammetry, 1980)*. But the value of Δp for a contour interval is weak: for example, the probable error in the contour lines can be about 10 percent of the contour interval because of lack of photographic resolution. Consequently, by increasing the size of Δp, the relative accuracy increases. Equation (3.1) shows the parallax is almost directly proportional to f and B, and inversely proportional to H. Thus, to increase p, f and/or B can be increased, and/or H can be decreased. But to increase f necessitates an increase in film size in order to have the same ground coverage if the value of B is to remain the same; to increase B necessitates a lens of wider angular field of view for the same reason; to decrease H necessitates a larger number of photographs of a given area which in turn, requires more field control stations.

A practical balance of the values of these elements, together with a consideration of map accuracy requirements, poses one of the most difficult economic problems in photogrammetry.

3.1.2.2 Horizontal uncertainty

When working on a plotting instrument, small differential changes in the projector position and angular orientation may cause

changes dX and dY in the coordinates of a point in the projection plane. The changes in the planimetric coordinates of a right-handed system due to db_x, db_y, db_z, $d\omega$, $d\phi$, $d\kappa$ given by *(Moffit et al., 1980)* are:

For the left projector:

$$dX' = db'_x + \frac{X}{h} db'_z + \frac{XY}{h} d\omega' - h\left(1 + \frac{X^2}{h^2}\right) d\phi' - Yd\kappa' \quad (3.9)$$

$$dY' = db'_y + \frac{Y}{h} db'_z + h\left(1 + \frac{Y^2}{h^2}\right) d\omega' - \frac{XY}{h} d\phi' + Xd\kappa' \quad (3.10)$$

Similarly for the right projector

$$dX'' = db''_x + \frac{(X - b)}{h} db''_z + \frac{(X - b)Y}{h} d\omega'' - h\left[1 + \frac{(X - b)^2}{h^2}\right] d\phi''$$

$$- Yd\kappa'' \quad (3.11)$$

$$dY'' = db''_y + \frac{Y}{h} db''_z + h\left(1 + \frac{Y^2}{h^2}\right) d\omega'' - \frac{(X - b)Y}{h} d\phi''$$

$$+ (X - b)\, d\kappa'' \quad (3.12)$$

Furthermore if eq. (3.11) is subtracted from that of eq. (3.9), the result is:

$$dX = dX' - dX'' = dp_x$$

The quantity dp_x can be used also to study the effect of differential projector motions on the elevations of points in the stereoscopic model.

The equations for dY given in eq. (3.10) and (3.12) are most important since relative orientation involves the elimination of y-parallax in the model ($dY' - dY'' = p_y$).

3.2 Determination of Movements by Mathematically Defined Object Points

A digital elevation model (DEM) can be formed for each observed epoch, based on the assumption that surface subsidence is primarily a vertical movement. The given rectangular surveying grid is superimposed on the area of interest, utilizing the software capabilities of the analytical plotter. The planimetric coordinates of grid points are set while the elevation is measured. A visit points routine or a digital terrain model program provided for analytical plotters drives the floating mark in a preplanned x,y pattern and the operator is required to keep the mark on the ground at specific stopping points.

The subsidence is represented as vertical movement vectors, which are calculated directly as differences between the elevations of the DEM's (Figure 3.1)

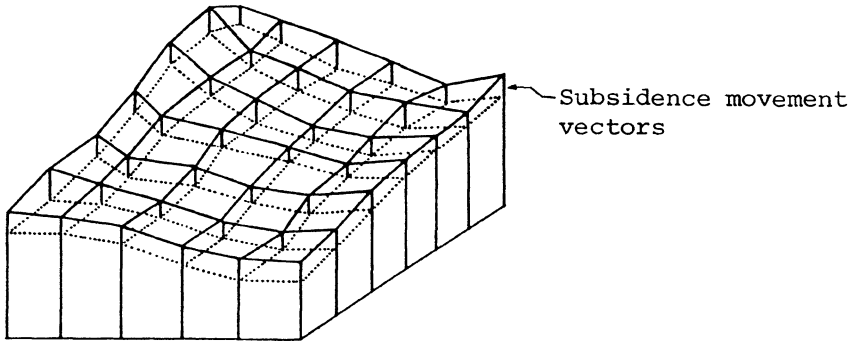

____ Initial digital elevation model

.... Deformed digital elevation model

Figure 3.1: Subsidence movement vectors from DEM's.

This type of approach has been successfully applied in open pit mining *(Toomey, 1982)* and volume determination *(Fenton, 1982; Johnson et al., 1982)* as well as in subsidence areas on flat terrain. In this process, stereomodels from the base photography are scanned and elevations digitized at regular grid points. Stereomodels from subsequent sets of photography are scanned in the identical manner, and volume differences are computed between the two digital elevation models. Use of the grid permits volume changes to be produced for different areas within the photography and changes may also be broken down to accurate elevation differences. Accuracy of volumes taken by digital terrain models using 1/6000 photography can be better than two percent. For further processing digital mapping techniques (i.e., digital data file, etc.) can be adapted for a rapid turnaround of data and greater flexibility of subsequent design decisions.

Although this technique has many advantages, it can be affected by the surface topography. In terrain with large slopes, subsidence may be accompanied by a large component of horizontal movements. By using fixed planimetric positions this fact is neglected, which leads to measured elevation of different points. Figure (3.2) illustrates these incorrect values, where the resulting Z component is smaller at all points except for point 5 due to surface topography.

3.3 Determination of Movements by Physically Defined Object Points

When targetted points are not available or when it is difficult to establish them, discrete natural points must be chosen

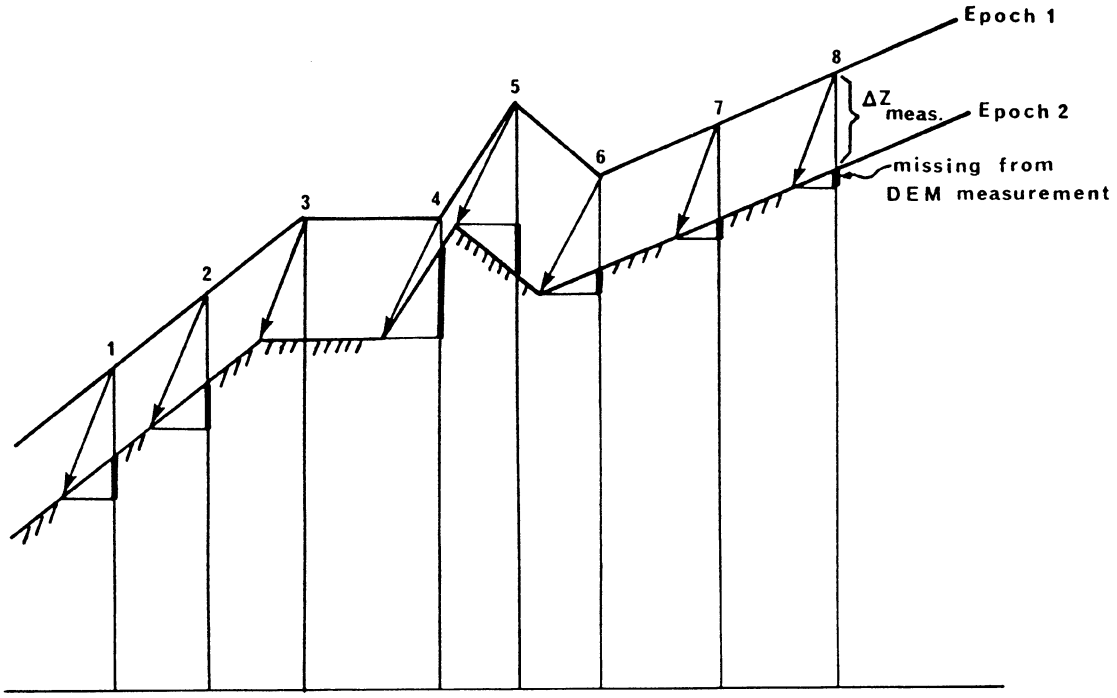

Figure 3.2: Incorrect Z-component of a DEM due to sliding.

for the determination of the movement vectors. To overcome the problem of point identification between two periods of measurements, a "cross-identification" procedure - described next - can be applied to facilitate the measurements of photo-coordinates.

The absolute object coordinates of the physically defined points can be calculated from bundle adjustment programs. The coordinate differences between two epochs directly represent the component of the displacements in the three coordinate directions.

Natural points are used also in the direct determination of the displacement vectors.

3.3.1 Cross-identification method

For the photogrammetric determination of displacements taking place over a long period of time, measurements must be performed on the same clearly identified photo-images of discrete points.

The time lapse between epochs, however, often makes point identification quite difficult, both in regard to absolute identification with respect to remembering just which points were measured earlier. Targetted points would be ideal, but require far too much effort, especially in mountainous terrain to be economically feasible, not to mention the difficulty of keeping them in place over a long period of time. Also, depending on the area, inclement weather conditions and curious wildlife virtually guarantee a high rate of loss. To overcome these difficulties a "cross-identification" method for the photo-measurements can be applied. In literature a relative procedure for terrestrial photographs can be found in *(Dauphin et al., 1977)*.

Let us assume that a stereopair of aerial photographs has been taken at epoch t_1, and later another stereopair at epoch t_2. In the "cross-identification" measuring procedure the left diapositive of epoch t_1 is set on to the left picture-carrier of a point transfer and marking instrument. On the right picture-carrier the right diapositive of epoch t_2 is set. Then the same image points can be identified and marked on both diapositives. To preserve stereoscopic perception the modern point marking instruments allow for optical image rotation and zoom magnification. Therefore, corresponding image points from photography of different scales can be accommodated.

The method, shown in Figure 3.3 has three advantages:

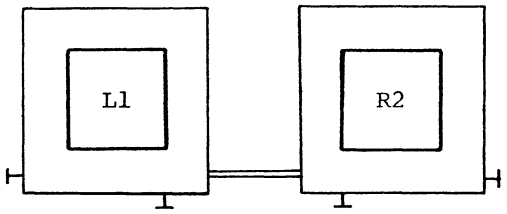

L1: Left diapositive of epoch t_1 .

R2: Right diapositive of epoch t_2 .

Figure 3.3: Arrangement of Cross-Identification Measuring Procedure.

-- First the points are marked permanently on both diapositives with high precision, under stereoscopic control, for further processing.

-- Secondly it verifies that the points appear on the photographs in both epochs. That is, if a point chosen in the first epoch has been annihilated during the period of time between the two epochs, one is not tempted into a false reading on some other point but may immediately choose a new point in the vicinity of the previous one and use this one in both periods.

-- Thirdly it facilitates the measurement procedure of the photo-coordinates on the stereocomparator. Since the points are marked on one diapositive of each epoch, their stereo identification is easily achieved with the matching diapositive of the same epoch.

3.4 Actual Object Displacements from Model Coordinate Differences

Being interested in the displacements of the points rather than in their absolute position, combined with the difficulties of resurveying the ground control points before each flight due to difficult

topographical conditions, led to the following method for determining displacements. First, the model displacement vectors are derived and from these, the object vectors in the three coordinate directions are determined.

For this purpose, relative orientation of model epoch 1 is performed analytically using the coplanarity condition (eq. 3.46) to define the five unknown parameters. Then the model coordinates of epoch 1 can be calculated according to eq. (3.68). Let these coordinates be:

$$[X_{M1} \quad Y_{M1} \quad Z_{M1}]^T_i \tag{3.13}$$

Then an absolute orientation of that model is done by a spatial similarity transformation,

$$\begin{bmatrix} X_i \\ Y_i \\ Z_i \end{bmatrix}_G = sR_{(\Omega,\Phi,K)} \begin{bmatrix} X_{M1} \\ Y_{M1} \\ Z_{M1} \end{bmatrix}_i + \begin{bmatrix} X_T \\ Y_T \\ Z_T \end{bmatrix} \tag{3.14}$$

where

$[X_i \; Y_i \; Z_i]^T_G$ = ground coordinates of point i

$[X_{M1} \; Y_{M1} \; Z_{M1}]^T_i$ = model coordinates of point i in epoch 1

$[X_T \; Y_T \; Z_T]^T$ = translation vector

$R_{(\Omega, \Phi, K)}$ = rotation matrix

s = uniform scale factor along the three axes directions.

In order to compute the seven unknown parameters ($s, \Omega, \Phi, K, X_T, Y_T, Z_T$) at least seven non-linear equations are required. Any model point whose three ground coordinates are known yields three equations

which in the expanded functional form of eq. (3.14) are:

$$F_1 = X_{P_G} - s\,(r_{11}\,X_{M1} + r_{21}\,Y_{M1} + r_{31}\,Z_{M1}) - X_T = 0$$

$$F_2 = Y_{P_G} - s\,(r_{12}\,X_{M1} + r_{22}\,Y_{M1} + r_{32}\,Z_{M1}) - Y_T = 0$$

$$F_3 = Z_{P_G} - s\,(r_{13}\,X_{M1} + r_{23}\,Y_{M1} + r_{33}\,Z_{M1}) - Z_T = 0 \qquad (3.15)$$

where the elements r_{ij} of the rotation matrix are:

$$r_{11} = \cos\Phi \cos K$$

$$r_{12} = \cos\Omega \sin K + \sin\Omega \sin\Phi \cos K$$

$$r_{13} = \sin\Omega \sin K - \cos\Omega \sin\Phi \cos K$$

$$r_{21} = -\cos\Phi \sin K$$

$$r_{22} = \cos\Omega \cos K - \sin\Omega \sin\Phi \sin K$$

$$r_{23} = \sin\Omega \cos K + \cos\Omega \sin\Phi \sin K$$

$$r_{31} = \sin\Phi$$

$$r_{32} = -\sin\Omega \cos\Phi$$

$$r_{33} = \cos\Omega \cos\Phi \qquad (3.16)$$

Depending on the type of the available ground control points the upper two equations of (3.15) are used for horizontal control, the last equation of (3.15) for vertical controls and all of them for full control points. Thus, the minimum number of control points required is two horizontal and three vertical. Usually more than the minimum number of control points are available with which to solve for the seven parameters of the transformation. In such cases, the least squares method is used to obtain a best estimate of the unknown parameters. Equations (3.15) are of the form $F(\bar{X},L) = 0$ and have the following linearized form *(Wells et al., 1971)*,

$$A\hat{X} + BV + W = 0 \qquad (3.17)$$

in which the first design matrix A is formed by the partial derivatives

of F's with respect to the unknowns

$$ {}_{m}A_{7} = \begin{bmatrix} \frac{\partial F_1}{\partial s} & \frac{\partial F_1}{\partial \Omega} & \frac{\partial F_1}{\partial \Phi} & \frac{\partial F_1}{\partial K} & \frac{\partial F_1}{\partial X_T} & \frac{\partial F_1}{\partial Y_T} & \frac{\partial F_1}{\partial Z_T} \\ \frac{\partial F_2}{\partial s} & \frac{\partial F_2}{\partial \Omega} & \frac{\partial F_2}{\partial \Phi} & \frac{\partial F_2}{\partial K} & \frac{\partial F_2}{\partial X_T} & \frac{\partial F_2}{\partial Y_T} & \frac{\partial F_2}{\partial Z_T} \\ \frac{\partial F_3}{\partial s} & \frac{\partial F_3}{\partial \Omega} & \frac{\partial F_3}{\partial \Phi} & \frac{\partial F_3}{\partial K} & \frac{\partial F_3}{\partial X_T} & \frac{\partial F_3}{\partial Y_T} & \frac{\partial F_3}{\partial Z_T} \\ - & - & - & - & - & - & - \end{bmatrix} = [a_{ij}], \begin{matrix} i=1,m \\ j=1,7 \end{matrix} \quad (3.18) $$

the second design matrix B is formed by the partial derivatives of F's with respect to the observations

$$ {}_{m}B_{n} = \begin{bmatrix} \frac{\partial F_1}{\partial X_{M1}} & \frac{\partial F_1}{\partial Y_{M1}} & \frac{\partial F_1}{\partial Z_{M1}} & \cdots \\ \frac{\partial F_2}{\partial X_{M1}} & \frac{\partial F_2}{\partial Y_{M1}} & \frac{\partial F_2}{\partial Z_{M1}} & \cdots \\ \frac{\partial F_3}{\partial X_{M1}} & \frac{\partial F_3}{\partial Y_{M1}} & \frac{\partial F_3}{\partial Z_{M1}} & \cdots \\ - & - & - & \cdots \end{bmatrix} = [b_{ij}], \begin{matrix} i=1,m \\ j=1,n \end{matrix} \quad (3.19) $$

the solution vector $\hat{X}$ is

$$ {}_{7}\hat{X}_{1} = [\delta s,\ \delta\Omega,\ \delta\Phi,\ \delta K,\ \delta X_T,\ \delta Y_T,\ \delta Z_T]^T \quad (3.20) $$

the residual vector V is

$$ {}_{n}V_{1} = [V_{XM1}\ \ V_{YM1}\ \ V_{ZM1}\ ,\ \ldots,\ V_{ZM_m}]^T \quad (3.21) $$

and the misclosure vector W is,

$$ W_1 = [F_1^o \quad F_2^o \quad F_3^o \quad \ldots \quad F_m^o]^T \quad (3.22) $$

where

$$m = 2H_Z + V_R, \quad n = 3(H_Z + V_R) \tag{3.23}$$

H_Z = number of horizontal control points

V_R = number of vertical control points.

The superscript (o) indicates that W is the value of the functions F computed first from initial approximate values of the seven unknown parameters and updated after each iteration. The first approximate values are computed as follows.

The scale factor, s^o, is given by the ratio of the horizontal distance between two control points on the ground and their corresponding distance in the model

$$s^o = \sqrt{(\Delta X_G^2 + \Delta Y_G^2)} \; / \; \sqrt{(\Delta X_M^2 + \Delta Y_M^2)} \tag{3.24}$$

The rotation angles Ω and Φ can initially be assumed to be zero (vertical photography). The initial value of K can be computed as,

$$K^o = \arctan (\Delta Y_G/\Delta X_G) - \arctan (\Delta Y_M/\Delta X_M) \tag{3.25}$$

while the initial translations are given as

$$X_T = \frac{\sum_{i=1}^{H_Z} X_i}{H_Z}, \qquad Y_T = \frac{\sum_{i=1}^{H_Z} Y_i}{H_Z}, \qquad Z_T = \frac{\sum_{i=1}^{V_R} Z_i}{V_R} \tag{3.26}$$

where

$$X_i = X_G^i - s^o(X_{M1}^i \cos K^o - Y_{M1}^i \sin K^o) \tag{3.27}$$

$$Y_i = Y_G^i - s^o(X_{M1}^i \sin K^o + Y_{M1}^i \cos K^o) \tag{3.28}$$

$$Z_i = Z_G^i - s^o Z_{M1}^i \tag{3.29}$$

The partial derivatives for the formation of A and B are derived in Appendix I.

With the matrices A, B, and W evaluated at the initial set of approximations, the values of the first set of corrections $\hat{X}$ are computed as *(Wells et al., 1971)*.

$$\hat{X} = - (A^T(BP^{-1}B^T)^{-1}A)^{-1}A^T(BP^{-1}B^T)^{-1}W \qquad (3.30)$$

where

P : is the weight matrix.

The corrections are added to the original approximations of the seven parameters to obtain a new set of approximations. These updated approximate values are then used to evaluate new values for the matrices A, B, W, which in turn are used to compute the new $\hat{X}$. In general then, the approximation $X_i^{(o)}$ at the end of the ith iteration may be computed from

$$X_i^{(o)} = X_{i-1}^{(o)} + \hat{X}_i \qquad (3.31)$$

At the end of each iteration a check is performed to see if it is necessary to continue with another iteration or to terminate the process. This check is usually performed according to different criteria of tolerance *(Mikhail, 1976; Ghosh, 1975)*. In this case 10^{-5} rad was chosen for the rotations and 1 mm for the translations. The number of iterations depends on the initial approximations, the unknown parameters, the geometric strength of the solution and the desired precision.

The evaluation of the accuracy of the solution is performed by computing the residuals $\hat{V}$, the a posteriori variance factor $\hat{\sigma}_o^2$ and the variance-covariance matrix Q of the unknown parameters as *(Wells et al., 1971)*

$$\hat{V} = - P^{-1}B^T(BP^{-1}B^T)^{-1}(A\hat{X} + W) \qquad (3.32)$$

$$\hat{\sigma}_o^2 = \frac{\hat{V}^T P \hat{V}}{df} \quad , \quad df = m - 7 \tag{3.33}$$

$$Q = \hat{\sigma}_o^2 \, (A^T (B P^{-1} B^T)^{-1} A)^{-1} \tag{3.34}$$

After the seven parameters have been computed with the help of the available control points, the scale and the rotations are stored for further processing. Computation of the object coordinates from model coordinates of, epoch t_1 is optional.

Subsequently, the model coordinates of epoch t_2 are computed, after the relative orientation parameters have been defined. These coordinates are:

$$[X_{M2} \quad Y_{M2} \quad Z_{M2}]^T \tag{3.35}$$

Then, a seven parameter spatial similarity transformation is utilized to transfer model epoch 2 to the model coordinate system of model epoch 1. Reference points i.e., points which appear in both models but are not affected by subsidence are used to determine the transformation parameters $(\lambda, \Omega_M, \Phi_M, K_M, X_{oM}, Y_{oM}, Z_{oM})$, using eq. (3.14). The main difference is in the formation of the design matrix B and the matrix of residual V. Here B consists of two submatrices. Since the model points of epoch t_1 can have a covariance matrix, they are treated as observations. Therefore,

$$[2H_Z + V_R]^B [6(H_Z + V_R)] = [B_1 \mid B_2] \tag{3.36}$$

and

$$B_1 = \frac{\partial F}{\partial L_1} \quad , \quad L_1 = \text{observation corresponding to model epoch 1}$$

$$B_2 = \frac{\partial F}{\partial L_2} \quad , \quad L_2 = \text{observations corresponding to model epoch 2}$$

Explicitly matrix B is given as,

$$
{}^{B}_{[2H_Z+V_R]\,[6(H_Z+V_R)]}
\begin{bmatrix}
\frac{\partial F_1}{\partial X_{M1}} & \frac{\partial F_1}{\partial Y_{M1}} & \frac{\partial F_1}{\partial Z_{M1}} & \frac{\partial F_1}{\partial X_{M2}} & \frac{\partial F_1}{\partial Y_{M2}} & \frac{\partial F_1}{\partial Z_{M2}} & \cdots \\
\frac{\partial F_2}{\partial X_{M1}} & \frac{\partial F_2}{\partial Y_{M1}} & \frac{\partial F_2}{\partial Z_{M1}} & \frac{\partial F_2}{\partial X_{M2}} & \frac{\partial F_2}{\partial Y_{M2}} & \frac{\partial F_2}{\partial Z_{M2}} & \cdots \\
\frac{\partial F_3}{\partial X_{M1}} & \frac{\partial F_3}{\partial Y_{M1}} & \frac{\partial F_3}{\partial Z_{M1}} & \frac{\partial F_3}{\partial X_{M2}} & \frac{\partial F_3}{\partial Y_{M2}} & \frac{\partial F_3}{\partial Z_{M2}} & \cdots \\
\cdots & \cdots & \cdots & \cdots & \cdots & \cdots & \cdots
\end{bmatrix} = [b_{ij}] \,, \qquad (3.37)
$$

where

$$i = 1,\ 2H_Z+V_R$$

$$j = 1,\ 6(H_Z+V_R)$$

and the partial derivatives are derived in the Appendix I, while

$$
{}^{6(H_Z+V_R)}V_1 = [V_{XM1_1}\ V_{YM1_2}\ V_{ZM1_3}\ V_{XM2_4}\ V_{YM2_5}\ V_{ZM2_6}\ \cdots\ V_{ZM2_{6(H_Z+V_R)}}]^T \qquad (3.38)
$$

In addition, every reference point provides three observation equations because its X_M, Y_M, Z_M model coordinates are known.

The solution is the iterative procedure of the combined case of least squares method and a description has already been given. The iterative procedure is terminated when the corrections for the rotations are less than 10^{-5} rad and for the translations less than 0.010 mm.

Once the seven parameters of eq. (3.14) are known, the points from model 2 are then transferred to the model 1 coordinate system using the same equation. At this stage every point - in the area of interest - influenced by subsidence will have two sets of coordinates,

since epoch 1 and 2 respectively refer to the same coordinate system. Obviously, the differences between each pair of coordinates represent the model displacement vectors due to subsidence,

$$\begin{bmatrix} dX_M \\ dY_M \\ dZ_M \end{bmatrix}_i = \begin{bmatrix} X^1_{M2} \\ Y^1_{M2} \\ Z^1_{M2} \end{bmatrix}_i - \begin{bmatrix} X_{M1} \\ Y_{M1} \\ Z_{M1} \end{bmatrix}_i \tag{3.39}$$

where

$[dX_M \; dY_M \; dZ_M]^T_i$ = model displacement vectors of point P_i

$[X_{M2} \; Y_{M2} \; Z_{M2}]^T_i$ = coordinates of point P_i of model 2 in model 1 coordinate system

$[Y_{M1} \; Y_{M1} \; Z_{M1}]^T_i$ = coordinates of point P_i in model 1.

Now the actual components of the displacements along three ground coordinate directions are obtained by applying the already stored 4-parameter transformation (scale and rotations), from the absolute orientation of model epoch 1, to the model displacement vectors (eq. 3.39). Explicitly, the ground displacement vectors are given by:

$$\begin{bmatrix} DX \\ DY \\ DZ \end{bmatrix}_i = s\,R_{(\Omega,\Phi,K)} \begin{bmatrix} dX_M \\ dY_M \\ dZ_M \end{bmatrix} \tag{3.40}$$

Figure (3.4), illustrates this procedure.

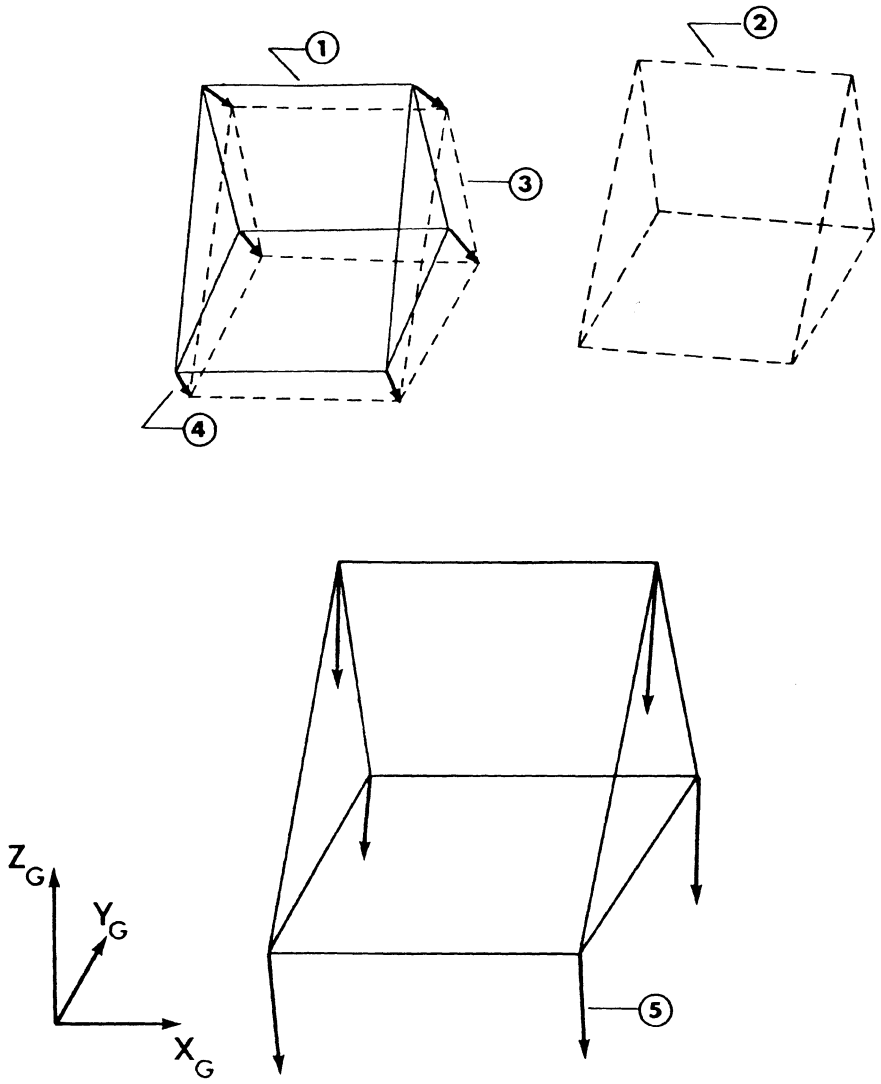

① Model 1

② Model 2

③ Model 2 in Model 1 coordinate system

④ Model displacement vectors

⑤ Ground displacement vectors

Figure 3.4: Ground displacement vectors from model coordinate differences.

The software for this approach has been developed by the author and tested on the University's IBM 370/3032 for a practical subsidence case in mountainous terrain.

The program:

1) Reads for both epochs:
   -- the fiducial marks of the four photographs (calibrated and measured)
   -- the photo points for relative orientation
   -- the natural points to be studied
   -- the basic interior orientation parameters x_o, y_o, f
   -- the coefficients of radial lens distortion
   -- the flying height and terrain ground elevation
   -- the reference points between model epoch 1 and model epoch 2
   -- the standard deviations of unit weight for photo and model coordinates
   -- the standard deviations of the observations.
2) Computes for both epochs:
   -- The refined image coordinates by:
      i - transferring the measured photo point, to the fiducial mark system
      ii - transferring to the photo system
      iii - applying corrections for radial lens distortion and atmospheric refraction (optional)
   -- The parameters of relative orientation, the photo residuals, the a posteriori variance factor and the variance-covariance matrix of the 5 unknowns
   -- The model coordinates and their residual parallaxes.

3) Computes for model epoch 1

   -- The parameters of the absolute orientation, the model residuals, the a posteriori variance factor, and the variance-covariance matrix of the seven unknowns

   -- The ground coordinates (optional)

4) Computes for model epoch 2

   -- The seven parameters to transfer it to model epoch 1 and the results of the least squares solution as mentioned previously

   -- the model coordinates of model epoch 2 in the model epoch 1 system

   -- the model coordinate differences

   -- the ground components of the displacements and the total vectors of displacements.

The software itself consists of the following parts to accomplish the aforementioned tasks.

MAIN : Reads some of the input information and calls the following subroutines:

PROTRA : Computes the eight projective transformation parameters

COTRA : Computes the transferred coordinates using the output from PROTRA

PHOCOR : Translates the photo points from the fiducial system to photo system

RALED : Eliminates the effect of radial lens distortion (optional)

ATREF : Performs the atmospheric refraction correction (optional)

RELOR : Computes the parameters of relative orientation

MODCRD : Computes model coordinates and residual parallaxes

PABSOR : Computes the parameters of absolute orientation of model epoch 1 with respect to the ground

M2TOM1 : Computes the parameters of transferring model epoch 2 to model epoch 1 coordinate system

TM2TM1 : Computes the transferred coordinates using the outputs from PABSOR and M2TOM1

MVED : Computes the model vectors of displacements

OVED : Computes the actual vectors of displacements and their total magnitude

COMADJ : Performs the combined case of the least squares adjustment

BINSER : Performs a binary search when is necessary. For example, to retrieve model coordinates of the reference points when their ID numbers are given.

Figure 3.5 depicts the flow of control through the program.

3.5 Measurement and Refinement of Image Coordinates

The objective of measurement and refinement of image coordinates is to determine the x and y coordinates of an image point with respect to the principal point, having eliminated the effects of systemmatic errors inherent in the photograph. There are three basic steps involved.

1 - The photo-coordinates are measured in a stereo-comparator in the reference system of the instrument.

2 - Transform the position of a point from machine axes system to fiducial axes system (photographic).

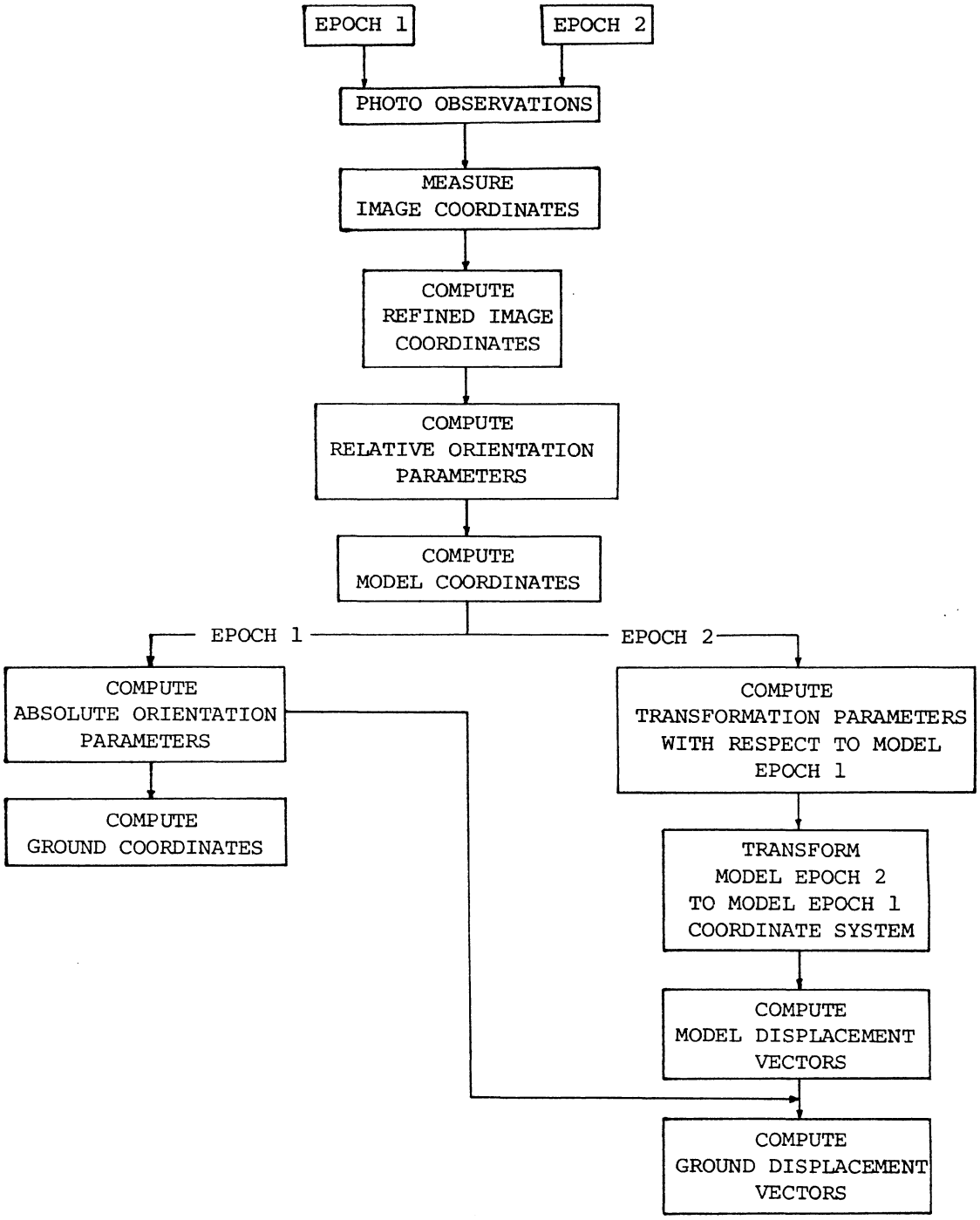

Figure 3.5: Flow of control of the developed software.

3 - Determine the correct position of a point by eliminating systematic errors such as

-- non-perpendicularity of stereo-comparator axes and film deformation

-- principal point displacement

-- lens distortion

-- atmospheric refraction.

3.5.1 Transformation to the fiducial coordinate system - correction for film and platen deformation

A projective or eight parameter transformation given by eq. (3.41) is used with four fiducial marks to transform the machine coordinates to the fiducial photo system *(Masry, 1978; Moffit et al., 1980)*. It allows corrections for linear film and platen deformations in any direction in the plane of the photograph.

$$X_F = \frac{a_1 X_M + b_1 Y_M + c_1}{a_3 X_M + b_3 Y_M + 1}$$

$$Y_F = \frac{a_2 X_M + b_2 Y_M + c_2}{a_3 X_M + b_3 Y_M + 1} \qquad (3.41)$$

where

X_M, Y_M : measured coordinates of the fiducial marks

X_F, Y_F : calibrated coordinates of the fiducial marks

a_1, ..., c_2 : unknown coefficients.

This transformation contains no redundancy with four fiducial marks (eight unknowns, requiring four non-collinear points

for a unique solution).

3.5.2 Transformation to the coordinate system of the photograph- Correction for principal point displacement

The camera calibration process determines the coordinates x_o and y_o of the principal point in the fiducial coordinate system. Thus, if the fiducial centre does not coincide with the principal centre the points must be further translated to the coordinate system of the photograph in order to place the origin at the principal point. The shifted photographic coordinates x_p and y_p of any point is then obtained as *(Moffit et al., 1982)*:

$$x_p = x_F - x_o$$
$$y_p = y_F - y_o \qquad (3.42)$$

where x_F, y_F are the coordinates in the fiducial system.

3.5.3 Correction for lens distortion

Radial lens distortion determined by lens calibration can be presented as an odd-powered polynomial *(American Society of Photogrammetry, 1980)* of the form:

$$\Delta r = k_1 r^3 + k_2 r^5 + k_3 r^7 + \ldots \qquad (3.43)$$

in which the k-coefficients are obtained by fitting the polynomial curve to the distortion data obtained from camera calibration by the method of least squares, and $r^2 = x_p^2 + y_p^2$.

The effect of lens distortion is eliminated by applying corrections to the photographic coordinates of the form

$$x_D = x_p \left(1 - \frac{\Delta r}{r}\right)$$

$$y_D = y_p \left(1 - \frac{\Delta r}{r}\right) \tag{3.44}$$

3.5.4 Correction for atmospheric refraction

Atmospheric refraction is one of the sources of errors which cause image distortion. If ΔR is the linear distortion on the image plane due to refraction, the corrected image coordinates are given from *(American Society of Photogrammetry, 1980)*

$$x = x_D \left(1 - \frac{\Delta R}{r}\right)$$

$$y = y_D \left(1 - \frac{\Delta R}{r}\right) \tag{3.45}$$

The derivation of ΔR is given in Appendix III.

3.6 Analytical Determination of the Relative Orientation Parameters

In the case of two photographs, there are two conjugate rays for each object point. Since these two rays originally emanate from the same object point at the time of photography, they must therefore be coplanar during any analytical solution as illustrated in Figure (3.6).

The corresponding mathematical condition, termed the coplanarity equation, enforces the fact that the two camera stations, the two image points, and the object point all lie on one and the same plane (epipolar plane). Analytically, the coplanarity equation is expressed by the scalar triple product *(American Society of Photogrammetry, 1980)*

$$\bar{B} \left(\bar{A}_i \times \bar{A}_j\right) = 0 \tag{3.46}$$

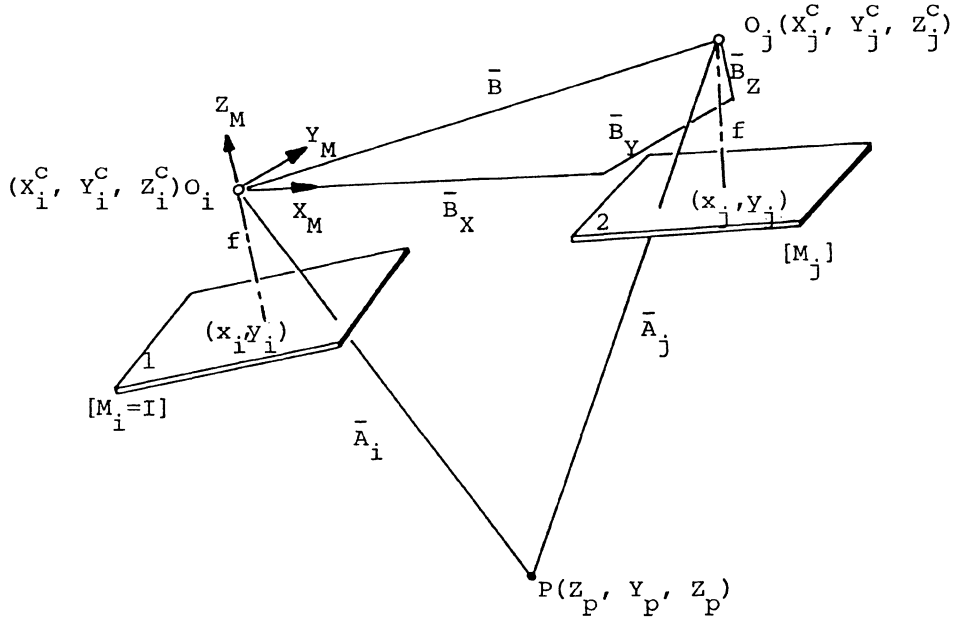

Figure 3.6: Relative orientation and coplanarity condition.

From Fig. (3.6) the vector $\bar{A}_i$ may be expressed in terms of its components as follows:

$$\bar{A}_i = (X_p - X_i^C)\bar{i} + (Y_p - Y_i^C)\bar{j} + (Z_p - Z_i^C)\bar{k} \tag{3.47}$$

and for refined image coordinates

$$\begin{bmatrix} X_p - X_i^C \\ Y_p - Y_i^C \\ Z_p - Z_i^C \end{bmatrix} = \lambda_i \, M_i \begin{bmatrix} x_i \\ y_i \\ -f \end{bmatrix} \tag{3.48}$$

where λ_i : is a scale factor

M_i : is the rotation matrix, with elements similar to eq. (3.16)

P : is a model point

Let

$$u_i = m_{11}x_i + m_{21}y_i + m_{31}(-f)$$
$$v_i = m_{12}x_i + m_{22}y_i + m_{32}(-f)$$
$$w_i = m_{13}x_i + m_{23}y_i + m_{33}(-f) \tag{3.49}$$

then eq. (3.48) becomes

$$\begin{bmatrix} X_p - X_i^c \\ Y_p - Y_i^c \\ Z_p - Z_i^c \end{bmatrix} = \lambda_i \begin{bmatrix} u_i \\ v_i \\ w_i \end{bmatrix} \tag{3.50}$$

Substituting eq. (3.50) into (3.47) we have for the left photograph

$$A_i = \lambda_i(u_i\bar{i} + v_i\bar{j} + w_i\bar{k}) \tag{3.51}$$

Similarly, for the right photograph

$$A_j = \lambda_j (u_j\bar{i} + v_j\bar{j} + w_j\bar{k}) \tag{3.52}$$

The base $\bar{B}$ may be expressed in terms of its components

$$\bar{B} = (X_j^c - X_i^c)\bar{i} + (Y_j^c - Y_i^c)\bar{j} + (Z_j^c - Z_i^c)\bar{k} \tag{3.53}$$

The coplanarity eq. (3.46) is expressed in determinant notation as:

$$F = \begin{vmatrix} B_x & B_y & B_z \\ A_i^i & A_i^j & A_i^k \\ A_j^i & A_j^j & A_j^k \end{vmatrix} = 0 \Rightarrow \lambda_i\lambda_j \begin{vmatrix} (X_j^c - X_i^c) & (Y_j^c - Y_i^c) & (Z_j^c - Z_i^c) \\ u_i & v_i & w_i \\ u_j & v_j & w_j \end{vmatrix} = 0 \tag{3.54}$$

or

$$(X_j^c - X_i^c)(v_iw_j - v_jw_i) - (Y_j^c - Y_i^c)(u_iw_j - u_jw_i) + (Z_j^c - Z_i^c)(u_iv_j - u_jv_i) = 0 \tag{3.55}$$

In the analytical solution the left-hand camera station is taken as the origin of an arbitrary coordinate system. Then $X_i^c = Y_i^c = Z_i^c = 0$, $\omega_i = \phi_i = \kappa_i = 0$, and $M_i = I$. Furthermore an

arbitrary value b_x^o is designated for the base component B_x.

Therefore the unknowns are $(Y_j^c - Y_i^c) = B_Y$, $(Z_j^c - Z_i^c) = B_Z$, $(\omega_j - \omega_i) = \omega_j''$, $(\phi_j - \phi_i) = \phi_j''$, $(\kappa_j - \kappa_i) = \kappa_j''$ and the refined photo coordinates x_i, y_i, x_j, y_j are measured quantities.

Since each pair of conjugate image points gives one coplanar equation, at least five pairs of conjugate image points need to be measured. Of course, the coplanarity equation (3.55) is non-linear and must first be linearized before it can be used for the solution of the unknown parameters. In addition, when more than five pairs of image coordinates are measured, the method of least squares is used to determine the most probable solution.

The coplanarity equation expressing the relationship between the measured quantities and the unknown parameters has the general form $F(\bar{X},L) = 0$. Therefore, the linearized form is given as follows *(Wells et al., 1971)*

$$A\hat{X} + BV + W = 0 \tag{3.56}$$

where

$_nA_5$: the first design matrix of the partial derivatives of F with respect to the five unknown parameters

$_5\hat{X}_1$: vector of corrections for the five specified unknown parameters

$_nB_{4n}$: the second design matrix of the partial derivatives of F with respect to the measured quantities

$_{4n}V_1$: the vector of the observational residuals

$_nW_1 = F(X^o,L)$: the misclosure vector

n : number of observed pairs of conjugate points.

The derivation of the partial derivatives is given in

Appendix II, while the final form of the system (3.56) is:

$$\begin{bmatrix} a_{11} & \cdots & a_{15} \\ \vdots & & \vdots \\ a_{n1} & \cdots & a_{n5} \end{bmatrix} \begin{bmatrix} \delta B_Y \\ \delta B_Z \\ \delta\omega''_j \\ \delta\phi''_j \\ \delta k''_j \end{bmatrix} + \begin{bmatrix} B_{11} & 0 & \cdots & 0 \\ 0 & B_{22} & & \vdots \\ \vdots & & \ddots & 0 \\ 0 & \cdots & 0 & B_{n,4n} \end{bmatrix} \begin{bmatrix} V^1_{x_i} \\ V^1_{y_i} \\ V^1_{x_j} \\ V^1_{y_j} \\ \vdots \\ V^n_{x_i} \\ V^n_{y_i} \\ V^n_{x_j} \\ V^n_{y_j} \end{bmatrix} + \begin{bmatrix} W_1 \\ W_2 \\ \vdots \\ W_n \end{bmatrix} = 0 \qquad (3.57)$$

where

$$B_{ij} = (b_{n,4n-3} \quad b_{n,4n-2} \quad b_{n,4n-1} \quad b_{n,4n}) \qquad (3.58)$$

The solution of the least squares for the unknown parameters is similar to the one given in section (3.6). The initial approximate values for the five unknowns are zero and the iterative procedure is terminated when the corrections for the rotations are less than 10^{-5} rad and for the base components less than 0.010 mm.

3.7 Calculation of Model Coordinates

The condition for relative orientation of a photo-pair is the intersection of five, evenly distributed, pairs of rays, $\bar{A}_1$ and $\bar{A}_2$. The two rays from a pair of conjugate images will, in general, not intersect in a model point, i.e., there may be residual parallaxes because of small unavoidable errors (Observational errors, systemmatic

errors, residual lens distortion, etc.).

Since the parameters of relative orientation have been computed, the coordinates of model points can be derived from either the left or the right photographs. Because of the non-intersection of the two conjugate rays, an acceptable procedure to define a point which will represent the location of the intersection, is usually the midpoint of vector $\bar{e}$ of the minimum distance between the two rays (Figure 3.7). The line segment $\bar{e}$ is called the common perpendicular of the two skew rays A_1, A_2.

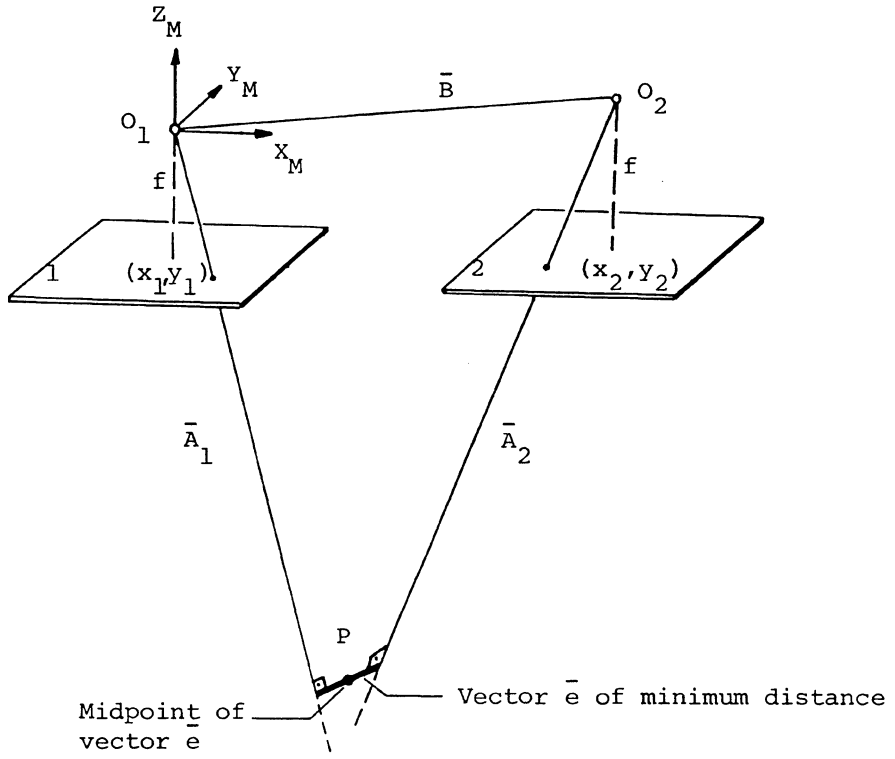

Figure 3.7: Non-intersection in coplanarity condition.

The direction (but not the length) of vector $\bar{e}$ is normal to both rays and is therefore given by their vector product *(Chosh, 1975)*

$$\bar{e} = \bar{a}_1 \times \bar{a}_2 \tag{3.59}$$

which can be written in the form

$$e = (v_1 w_2 - w_1 v_2)\bar{i} - (u_1 w_2 - w_1 u_2)\bar{j} + (u_1 v_2 - v_1 u_2)\bar{k} \tag{3.60}$$

or

$$\bar{e} = \begin{bmatrix} e_x \\ e_y \\ e_z \end{bmatrix} = \begin{vmatrix} \bar{i} & \bar{j} & \bar{k} \\ u_1 & v_1 & w_1 \\ u_2 & v_2 & w_2 \end{vmatrix} \tag{3.61}$$

in which $\bar{i}$, $\bar{j}$, $\bar{k}$ are the unit vectors in X, Y, Z directions respectively and

$$\begin{bmatrix} u_1 \\ v_1 \\ w_1 \end{bmatrix} = \begin{bmatrix} x_1 \\ y_1 \\ -f \end{bmatrix}, \quad \begin{bmatrix} u_2 \\ v_2 \\ w_2 \end{bmatrix} = M_2 \begin{bmatrix} x_2 \\ y_2 \\ -f \end{bmatrix} \tag{3.62}$$

The components of $\bar{e}$ can be computed because all the quantities on the right-hand side of eq. (3.61) are known. In order to determine the position of the $\bar{e}$-vector relative to O_1 and O_2, the vectors $\bar{a}_1$, $\bar{a}_2$ and $\bar{e}$ must be properly scaled by scalars λ_1, λ_2, and d respectively. It follows directly from Fig. (3.7) that the vector polygon containing these scaled vectors together with the base vector $\bar{B}$ must close. That is,

$$\bar{B} = \lambda_1 a_1 + de - \lambda_2 a_2 \tag{3.63}$$

or in vector forms

$$\begin{bmatrix} B_x \\ B_y \\ B_z \end{bmatrix} = \begin{bmatrix} X^M_{02} \\ Y^M_{02} \\ Z^M_{02} \end{bmatrix} - \begin{bmatrix} X^M_{01} \\ Y^M_{01} \\ Z^M_{01} \end{bmatrix} = \lambda_1 \begin{bmatrix} u_1 \\ v_1 \\ w_1 \end{bmatrix} + d \begin{bmatrix} e_x \\ e_y \\ e_z \end{bmatrix} - \lambda_2 \begin{bmatrix} u_2 \\ v_2 \\ w_2 \end{bmatrix} \quad (3.64)$$

where λ_1, λ_2, d are three unknown scalar multipliers. From the above eq. (3.64) a system of three linear equations can be formed, thus

$$\begin{bmatrix} u_1 & e_x & -u_2 \\ v_1 & e_y & -v_2 \\ w_1 & e_z & -w_2 \end{bmatrix} \begin{bmatrix} \lambda_1 \\ d \\ \lambda_2 \end{bmatrix} = \begin{bmatrix} B_x \\ B_y \\ B_z \end{bmatrix} \quad (3.65)$$

The solution of the system is given by:

$$\lambda_1 = \frac{\begin{vmatrix} B_x & e_x & -u_2 \\ B_y & e_y & -v_2 \\ B_z & e_z & -w_2 \end{vmatrix}}{\begin{vmatrix} u_1 & e_x & -u_2 \\ v_1 & e_y & -v_2 \\ w_1 & e_z & -w_2 \end{vmatrix}} \quad d = \frac{\begin{vmatrix} u_1 & B_x & -u_2 \\ v_1 & B_y & -v_2 \\ w_1 & B_z & -w_2 \end{vmatrix}}{\begin{vmatrix} u_1 & e_x & -u_2 \\ v_1 & e_y & -v_2 \\ w_1 & e_z & -w_2 \end{vmatrix}} \quad \lambda_2 = \frac{\begin{vmatrix} u_1 & e_x & B_x \\ v_1 & e_y & B_y \\ w_1 & e_z & B_z \end{vmatrix}}{\begin{vmatrix} u_1 & e_x & -u_2 \\ v_1 & e_y & -v_2 \\ w_1 & e_z & -w_2 \end{vmatrix}} \quad (3.66)$$

The coordinates of a model point can be determined *(Moffit et al., 1980)* next as:

$$P = O_1 + \lambda_1 a_1 + (0.5)de \quad (3.67)$$

or in the vector form

$$\begin{bmatrix} X_M \\ Y_M \\ Z_M \end{bmatrix} = \begin{bmatrix} X^M_{01} \\ Y^M_{01} \\ Z^M_{01} \end{bmatrix} + \lambda_1 \begin{bmatrix} u_1 \\ v_1 \\ w_1 \end{bmatrix} + (0.5)d \begin{bmatrix} e_x \\ e_y \\ e_z \end{bmatrix} \quad (3.68)$$

The model positions of all of the measured points can thus be established.

Given arbitrary values to the coordinates of the perspective center O_1, the coordinates of the perspective center O_2 can be obtained by adding the components of the base $\bar{B}$ to O_1. Thus

$$\begin{bmatrix} X^M_{02} \\ Y^M_{02} \\ Z^M_{02} \end{bmatrix} = \begin{bmatrix} X^M_{01} \\ Y^M_{01} \\ Z^M_{01} \end{bmatrix} + \begin{bmatrix} B_x \\ B_y \\ B_z \end{bmatrix} \tag{3.69}$$

Because the midpoint of vector $\bar{e}$ has been selected arbitrarily we can say that the procedure for determining a space intersection given above is approximate. However, this approximation is quite acceptable for practical applications. The length of the common-perpendicular vector $\bar{e}$ between two conjugate rays is an indication of the extent by which the two rays miss intersecting each other. This length is called the residual parallax, and is given by

$$\begin{aligned} r_p &= d \cdot |\vec{e}| \\ &= d \cdot (e_x^2 + e_y^2 + e_z^2)^{1/2} \end{aligned} \tag{3.70}$$

4

ESTIMATED ACCURACIES

4.1 Accuracy Determination of the Photogrammetric Results

The displacement vectors ΔS_{ij} can be determined directly, as previously mentioned, from the absolute position of the object points in two different epochs as:

$$\Delta S_{p_{ij}} = (\Delta\hat{X}^2_{p_{ij}} + \Delta\hat{Y}^2_{p_{ij}} + \Delta\hat{Z}^2_{p_{ij}})^{1/2} \tag{4.1}$$

where:

$\Delta S_{p_{ij}}$ = displacement vector of point p

$$\Delta\hat{X}_{p_{ij}} = \hat{X}_{p_j} - \hat{X}_{p_i} \tag{4.2}$$

$$\Delta\hat{Y}_{p_{ij}} = \hat{Y}_{p_j} - \hat{Y}_{p_i} \tag{4.3}$$

$$\Delta\hat{Z}_{p_{ij}} = \hat{Z}_{p_j} - \hat{Z}_{p_i} \tag{4.4}$$

i: refers to epoch t_1

j: refers to epoch t_2.

The evaluation of the accuracy of $\Delta S_{p_{ij}}$ is based on the accuracy of the estimated solution vectors ${}_3\hat{X}_1$ for each epoch, which is expressed by the covariance matrices $\Sigma_{\hat{X}_i}$ and $\Sigma_{\hat{X}_j}$ respectively.

Expressing eq. (4.2) to (4.4) in vector form and applying the propagation of covariances, the accuracy of the components of the displacement vector along the three coordinate axes can be determined. Hence

$$\begin{bmatrix} \hat{\Delta X}_{ij} \\ \hat{\Delta Y}_{ij} \\ \hat{\Delta Z}_{ij} \end{bmatrix} = \begin{bmatrix} I & -I \end{bmatrix} \begin{bmatrix} \hat{X}_j \\ \hat{Y}_j \\ \hat{Z}_j \\ \hat{X}_i \\ \hat{Y}_i \\ \hat{Z}_i \end{bmatrix} \tag{4.5}$$

and eq. (4.4) can be written as:

$$_3\Delta X_1 = {}_3D_6 \; {}_6X_1 \tag{4.6}$$

which is a linear function.

The propagation of covariances is given *(Mikhail, 1976)* as:

$$C_{\Delta X} = D \, C_X \, D^T \tag{4.7}$$

The matrix D represents the Jacobian of ΔX with respect to X, and

$$C_X = \begin{bmatrix} \Sigma_{\hat{X}_j} & 0 \\ 0 & \Sigma_{\hat{X}_i} \end{bmatrix} \tag{4.8}$$

is the covariance matrix of X.

Applying the propagation of covariances to eq. (4.5), the accuracy of the components of the displacement vector is given from eq. (4.7) as:

$$C_{\Delta\hat{X}_{ij},\Delta\hat{Y}_{ij},\Delta\hat{Z}_{ij}} = \left[\frac{\partial\Delta\hat{X}_{ij},\Delta\hat{Y}_{ij},\Delta\hat{Z}_{ij}}{\partial\hat{X}_j,\hat{Y}_j,\hat{Z}_j,\hat{X}_i,\hat{Y}_i,\hat{Z}_i}\right] C_{\hat{X}_j,\hat{Y}_j,\hat{Z}_j,\hat{X}_i,\hat{Y}_i,\hat{Z}_i} \left[\frac{\partial\Delta\hat{X}_{ij},\Delta\hat{Y}_{ij},\Delta\hat{Z}_{ij}}{\partial\hat{X}_j,\hat{Y}_j,\hat{Z}_j,\hat{X}_i,\hat{Y}_i,\hat{Z}_i}\right]^T \tag{4.9}$$

which is equal to:

$$C_{\Delta\hat{X}_{ij},\Delta\hat{Y}_{ij},\Delta\hat{Z}_{ij}} = \begin{bmatrix} I & -I \end{bmatrix} \begin{bmatrix} \Sigma_{\hat{X}_j} & 0 \\ 0 & \Sigma_{\hat{X}_i} \end{bmatrix} \begin{bmatrix} I \\ -I \end{bmatrix} \tag{4.10}$$

3 x 3 3 x 6 6 x 6 6 x 3

and the final form of the variance-covariance matrix of the components of the displacements is:

$$C_{\Delta\hat{X}_{ij},\Delta\hat{Y}_{ij},\Delta\hat{Z}_{ij}} = \Sigma_{\hat{X}_j} + \Sigma_{\hat{X}_i} \tag{4.11}$$

The accuracy of $\Delta S_{p_{ij}}$ can be examined either in one-dimensional test with respect to its standard deviation $\sigma_{\Delta S}$ or in three-dimensional test with respect to the error ellipsoid in $\Delta\hat{X}$, $\Delta\hat{Y}$, $\Delta\hat{Z}$ space. For the latter, the vector $\Delta S_{p_{ij}}$ is examined if it falls inside or on to the ellipsoid with a certain probability.

4.2 One-Dimensional Test

The variance $\sigma^2_{\Delta S}$ of the displacement vector can be determined by applying the error propagation law to eq. (4.1) and neglecting the covariances of $\Delta\hat{X}_{ij}$, $\Delta\hat{Y}_{ij}$ and $\Delta\hat{Z}_{ij}$ because they are small quantities.

Hence:

$$\sigma^2_{\Delta S_p} = \left(\frac{\hat{\Delta X}_{ij}}{\Delta S_{p_{ij}}}\right)^2 \sigma^2_{\hat{\Delta X}} + \left(\frac{\hat{\Delta Y}_{ij}}{\Delta S_{p_{ij}}}\right)^2 \sigma^2_{\hat{\Delta Y}} + \left(\frac{\hat{\Delta Z}_{ij}}{\Delta S_{p_{ij}}}\right)^2 \sigma^2_{\hat{\Delta Z}} \qquad (4.12)$$

Then, the ratio

$$\sigma_{\Delta S_{p_{ij}}} / \Delta S_{p_{ij}} \qquad (4.13)$$

will be used to determine the accuracy of the displacement vectors $\Delta S_{p_{ij}}$.

4.3 Three-Dimensional Test

Knowing the variance-covariance matrix $C_{\hat{\Delta X},\hat{\Delta Y},\hat{\Delta Z}}$ in the $\hat{\Delta X},\hat{\Delta Y},\hat{\Delta Z}$ space, the quadratic form,

$$[\hat{\Delta X}\ \hat{\Delta Y}\ \hat{\Delta Z}]\ C^{-1}_{\hat{\Delta X},\hat{\Delta Y},\hat{\Delta Z}}\ [\hat{\Delta X}\ \hat{\Delta Y}\ \hat{\Delta Z}]^T = c \qquad (4.14)$$

represents an equation of a tri-axial ellipsoid *(Wells et al., 1971)* centered at (0,0,0). It also has a χ^2-distribution with 3 degrees of freedom *(Mikhail, 1976)*.

It can be said now that a displacement has occured when the point p represented by the vector $\Delta S_{p_{ij}}$ lies outside the error ellipsoid. This happens when the value c, calculated from eq. (4.13), exceeds the value $\chi^2_{(1-\alpha),3}$, where α is the significance level.

The error ellipsoid and the displacement vector are illustrated in Figure 4.1.

A small program was written to perform both tests mentioned, where the input for each point is its coordinates in both epochs and their variance-covariance matrices. The output contains information

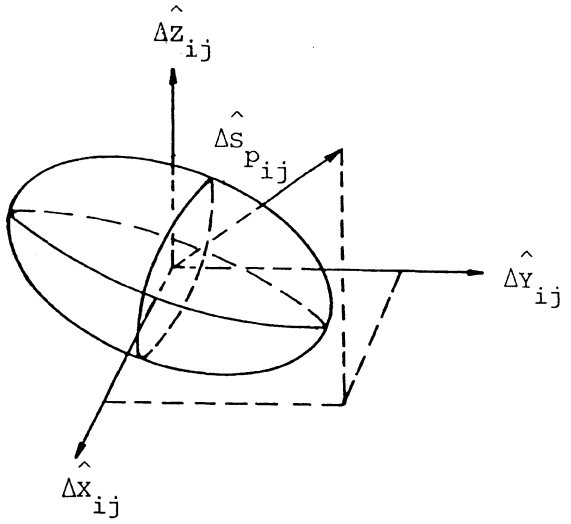

Figure 4.1: Error ellipsoid and displacement vector.

about the magnitude of the displacement vector at each point, the standard deviation, the accuracy (one-dimensional test), the value c of the quadratic form and if the displacement is significant at a certain probability level (three-dimensional test).

4.4 Test for Compatibility Between Photogrammetric and Surveying Results

The movement of every point affected by subsidence is expressed by its spatial displacement vector ΔS_p, computed between two epochs.

Photogrammetric results can be examined with respect to the ground surveying data by testing the compatibility of the two methods. In order to test the equality of two independent determinations of ΔS_p our null hypothesis is:

$$H_o : \Delta S_p^P = \Delta S_p^S \qquad (4.15)$$

where

ΔS_p^P : displacement vector of point p computed by photogrammetry

ΔS_p^S : displacement vector of point p computed by ground surveying techniques.

The null hypothesis H_o is tested by examining the differences between the approaches, which in vector form are:

$$\underset{n \quad 1}{[\Delta S_p^P]} - \underset{n \quad 1}{[\Delta S_p^S]} = \underset{n \quad 1}{[r_n]} \tag{4.16}$$

where

n : is the number of points

r_n : the differences between the two methods.

The ideal situation is when each $r_n = 0$ and thus the expectation of all r_n's is zero:

$$E(r_n) = \mu_r = 0 \tag{4.17}$$

This leads to multinormal populations, where, for two samples of independent observations with mean vectors ΔS_p^P and ΔS_p^S and common covariance matrix Σ, a multihypothesis H_o is tested by the following statistic *(Morrison, 1976)*:

$$\zeta = \frac{n_p n_S}{n_p + n_S} (\Delta S_p^P - \Delta S_p^S)^T \Sigma^{-1} (\Delta S_p^P - \Delta S_p^S) \tag{4.18}$$

where:

n_p, n_S : the sizes of the samples

Σ : covariance matrix of the population

$\Delta S_p^P, \Delta S_p^S$: the two samples.

With the covariance matrices of the samples known and given by:

$$C_i = \frac{1}{n_i} \Sigma_i \quad , \quad i = P,S \tag{4.19}$$

eq. (4.17) becomes:

$$\zeta = (\Delta S_p^P - \Delta S_p^S)^T \, C_{\Delta S_p}^{-1} \, (\Delta S_p^P - \Delta S_p^S) \tag{4.20}$$

where:

$C_{\Delta S_p}$: covariance matrix of the sample.

If H_o holds true, the quantity of eq. (4.20) has a χ^2-distribution with u degrees of freedom (u = rank ($C_{\Delta S_p}$)). It is possible now to define 100 (1-α)% confidence intervals, where α is the level of significance.

Therefore H_o is accepted when:

$$0 < \zeta < \xi_{\chi^2_{u,1-\alpha}} \tag{4.21}$$

5

PRACTICAL APPLICATION

5.1 Description of the Area

The photogrammetric approaches were studied at a test area in the Rocky Mountains, where aerial photographs were taken before commencement of the exploitation, and again after a coal seam panel had been extracted. A planimetric map of the subsidence study area is illustrated in Figure (5.1) showing the mountainous terrain.

The coal seam is rather thick with a steep dip angle. The surface terrain rises steeply from the outcrop of the seam thus resulting in a rapid change of cover depth above the exploitation panels. The coal seam is extracted at its entire thickness using a hydraulic* mining method causing roof cavings. A cross-section of the mining area is shown in Figure (5.2).

The area is ideal for photogrammetric test as a past forest fire followed by avalanches has left the slope with sparce vegetation and no trees. Furthermore, there is a number of geodetic surveying stations in the area as well as rock mechanics instrumentation (tiltmeters) for absolute reference and checking *(Fisekci et al., 1981)*.

---

* Description of the method is given in Appendix IV.

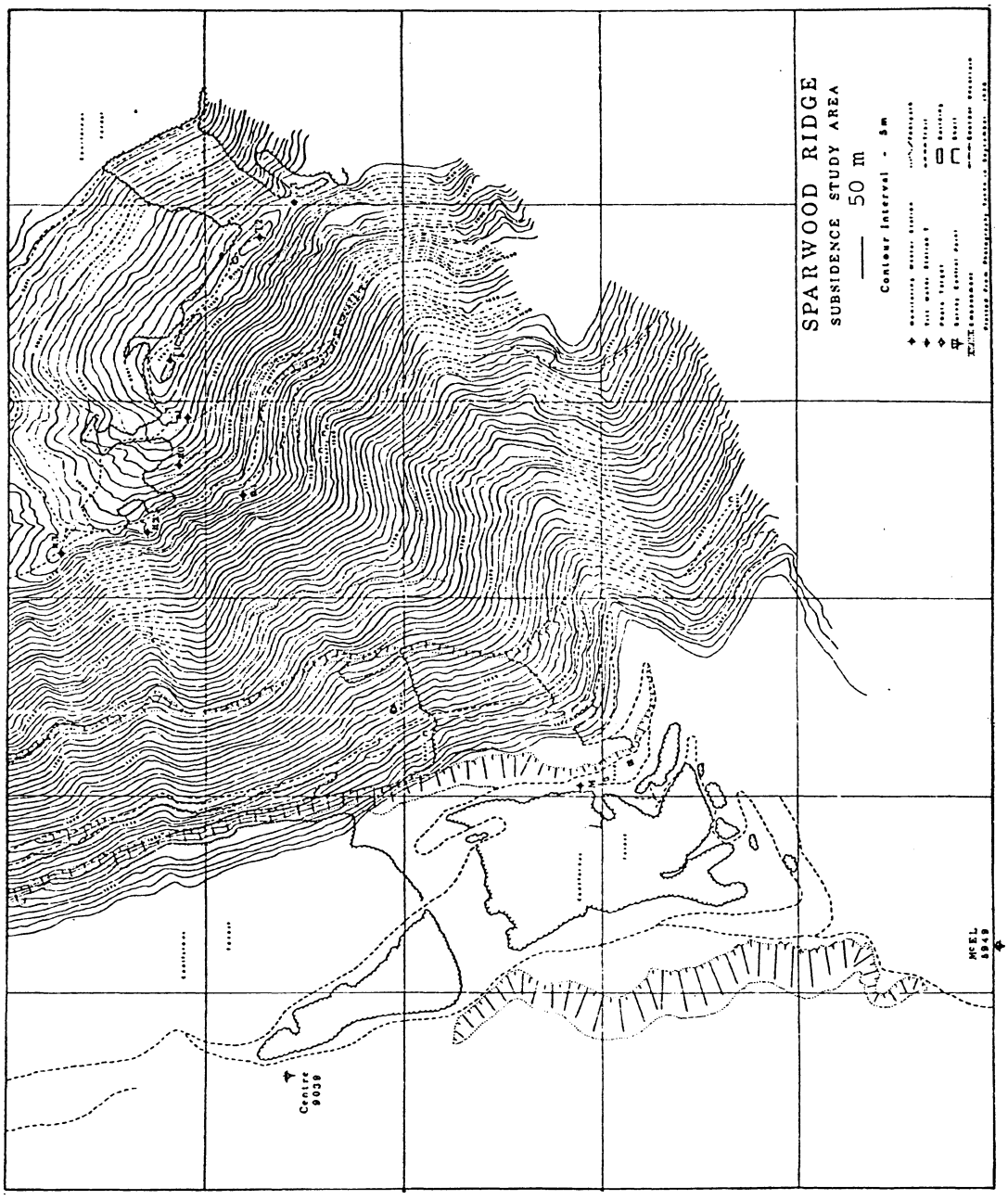

Figure 5.1: Planimetric map of the study area.

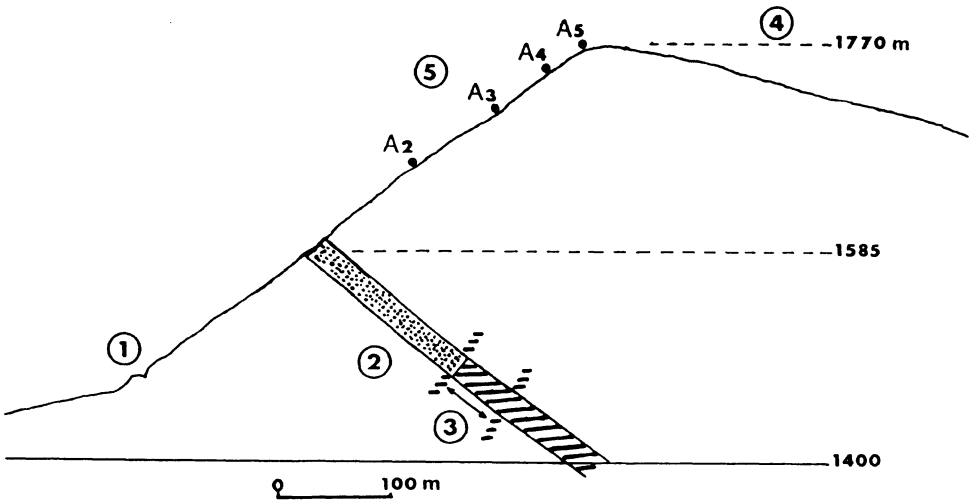

Figure 5.2: Cross-section of the mining area.
1) haul road; 2) exploited area; 3) planned exploitation;
4) ground elevation; 5) physical subsidence stations.

5.2 Results of the Tests

a) Using aerial photographs of the two epochs, a map in 1/2500 scale with 5 metres contour interval was compiled for each epoch. A comparison of the two map manuscripts showed that the changes were not significantly large to justify production of a subsidence contour map. However, there were a number of fractures, holes, etc., which were plotted. The reasons for the unsatisfactory interpretation are:

   i) the accuracy of the contour lines

   ii) the steepness of the slope which causes sliding as well as vertical subsidence.

b) The analytical plotter AP-2C (O.M.I.) and mathematically defined points were used to monitor subsidence based on the principle of

Digital Elevation Models. The model of the test area was formed and then elevations of the same grid points and profiles for each epoch were measured. Although it was expected that the subsidence vector could be calculated as the difference between the elevations of the same grid point of the two epochs, the results were not at the level of accuracy which was required. The horizontal component of the movement was unexpectedly large so that different surface points were corresponding to the same fixed planimetric position. Some improvement may be obtained by shifting the grid by the average horizontal movement - in opposite direction. However, due to terrain relief and to different underground activities the sliding of the slope shows large descrepancies from place to place, render this correction useless for practical purposes.

c) Aerial photographs of each individual epoch were used to determine absolute coordinates of natural points. The analytical plotter AP-2C (O.M.I.) was used again in comparator mode to measure the photo-coordinates of the physically defined object points, which had been marked on the diapositives with the aid of the "cross-identification" method.

Two bundle adjustment programs with self-calibration, namely UNB-ASC2 *(Moniwa, 1977)* and GEBAT-V *(El-Hakim, 1982)* were used for the computation of the ground coordinates of each epoch. For having compatible results between epoch t_1 and epoch t_2 the control points were kept the same for both epochs.

The displacement vectors of a point were then calculated as the difference of the absolute coordinates. The final results of

the displacements were graphically illustrated. Plans were plotted, showing the horizontal location of the profiles using physical points, the deformation vectors within the individual profiles, the horizontal movement vectors (Figure 5.3) and the contours of equal subsidence (Figure 5.4).

In a first phase, the program UNB-ASC2 was used to provide ground coordinates for the measured photo-points and the parameters for the interior and absolute orientation of the camera stations. Next GEBAT-V was run which requires approximate values of the unknown parameters. The choice of GEBAT-V is based on the output information about the accuracy of the ground coordinates (it provides variance-covariance matrix for each point), which permits a statistical analysis of the results.

Statistical quantities for both epochs are given in Table 5.1.

The absolute accuracy of the displacements obtained by photogrammetry is determined by comparing these results with those from ground surveying techniques (Table 5.2).

In addition, Figure (5.3) shows a comparison between the horizontal movement vectors obtained from the two approaches.

The evaluation of the photogrammetric results was done according to the previously mentioned one- and three-dimensional tests.

Due to the steep slope and the unsatisfactory distribution of the control points, the accuracy was not uniform over the area. The performance of one-dimension test revealed a mean accuracy of $\sigma_{\Delta S}/\Delta S = 1/165.1$, while the standard deviation was

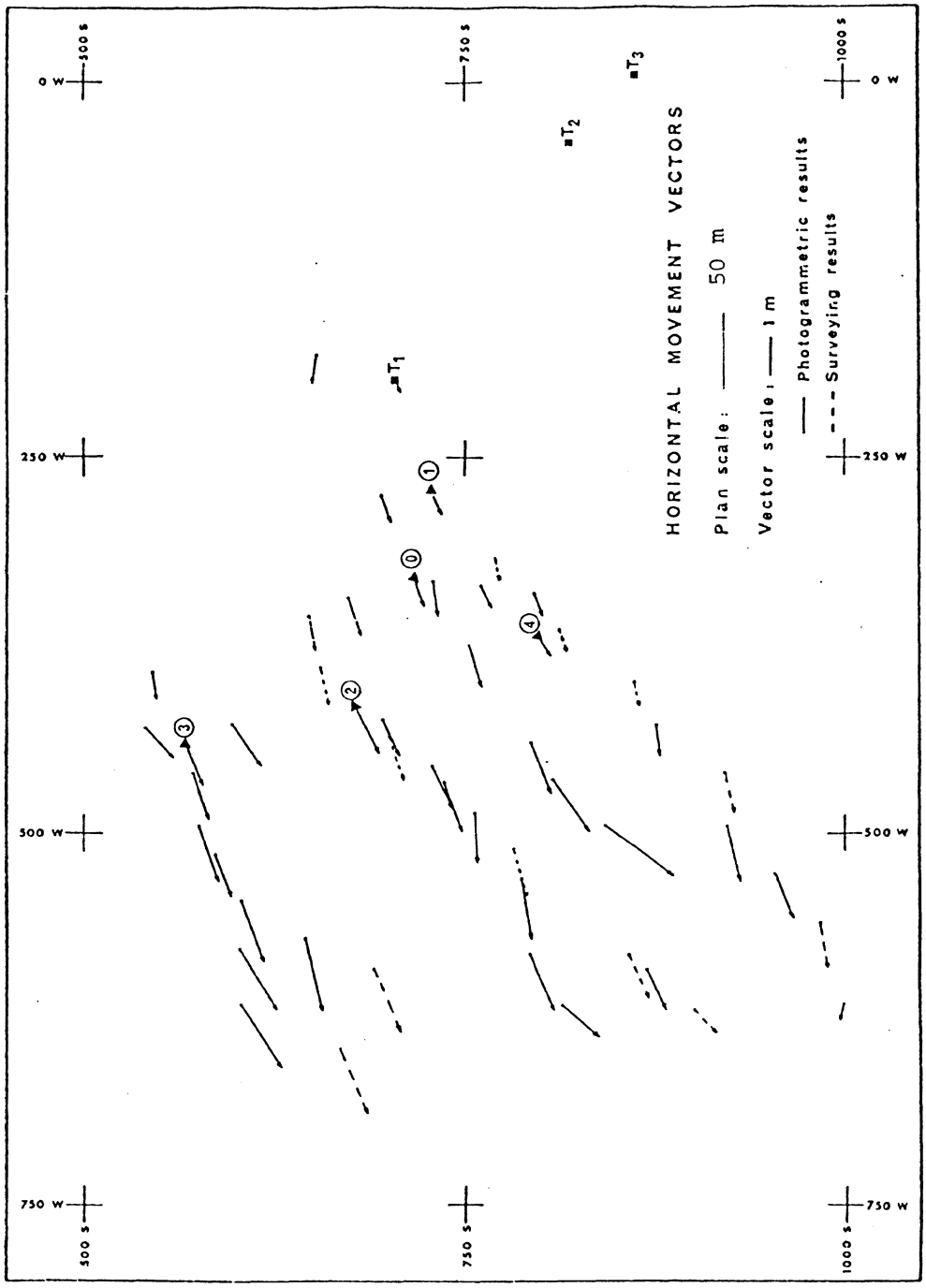

Figure 5.3: Horizontal movement vectors.

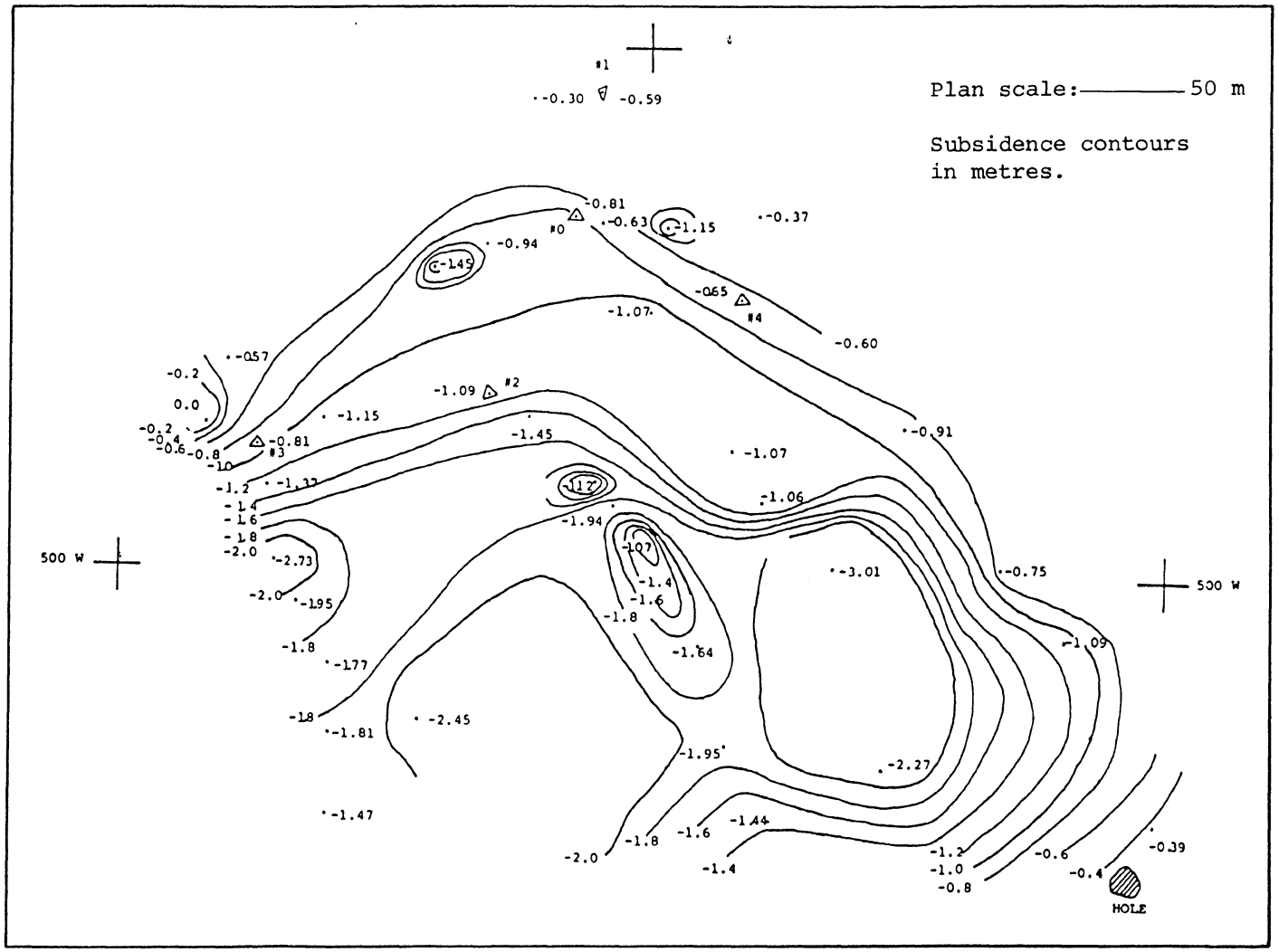

Figure 5.4: Contours of equal subsidence.

TABLE 5.1

Summary of bundle adjustment statistics.

		Epoch 1	Epoch 2
	RMS Vx_p	2.8 μm	4.0 μm
	RMS Vy_p	8.7 μm	10.6 μm
Resicuals of photo points			
	Mean Vx_p	-0.006 μm	-0.008 μm
	Mean Vy_p	-0.014 μm	-0.022 μm
Check point differences	RMS CHX	0.099 m	0.122 m
	RMS CHY	0.057 m	0.012 m
	RMS CHZ	0.033 m	0.121 m
	Mean $\bar{X}$	0.098 m	0.121 m
	Mean $\bar{Y}$	0.057 m	0.011 m
	Mean $\bar{Z}$	0.031 m	0.041 m
Means of all non-control points			
standard deviations	$\overline{RMS}$ X	0.036 m	0.035 m
	$\overline{RMS}$ Y	0.027 m	0.029 m
	$\overline{RMS}$ Z	0.084 m	0.103 m
Semi-major axes of the error	$\bar{a}$ X	0.055 m	0.070 m
ellipsoids at 0.95 confidence	$\bar{b}$ Y	0.081 m	0.088 m
region	$\bar{c}$ Z	0.238 m	0.284 m

TABLE 5.2

Movement vectors obtained by photogrammetry and by surveying ground techniques.

Point	ΔX(m)			ΔY(m)			ΔZ(m)		
No.	Photo	Survey	δX_{P-S}	Photo	Survey	δY_{P-S}	Photo	Survey	δZ_{P-S}
100	-0.81	-0.83	0.02	-0.38	-0.32	0.06	-0.71	-0.73	0.02
101	-0.70	-0.73	0.03	-0.32	-0.24	0.08	-0.50	-0.51	0.01
102	-1.27	-1.28	0.01	-0.64	-0.57	0.07	-1.14	-1.15	0.01
103	-1.10	-1.15	0.05	-0.64	-0.58	0.06	-0.96	-0.95	0.01
104	-0.68	-0.69	0.03	-0.44	-0.38	0.06	-0.59	-0.62	0.03

TABLE 5.3

Displacement vectors (m).

Point #	Photo	Survey	δ_{P-S}
100	1.14	1.15	-0.01
101	0.92	0.92	0.00
102	1.82	1.81	0.01
103	1.60	1.60	0.00
104	1.00	1.00	0.00

$\sigma_{\eta-1}(\sigma_{\Delta S}/\Delta S)$ = 1/105.4 (min 1/14.2 - max 1/451.3).

The three-dimensional test showed that displacement have occured, at 0.95 confidence level at all the points except one.

Photogrammetric and surveying results were not compared statistically due to the small size of the sample (only five surveying results were available). Hence the comparison was based on the Tables (5.2) and (5.3) when absolute values were compared for the first and second epoch.

For the third epoch the displacements were defined by the direct determination of actual movements from model coordinate differences. Indications of the achievable accuracies are given here by mean values and RMS of:

a) photo-residuals after relative orientation: $\bar{r}$ = 0.0 μm, σ_r = 2 μm

b) differences of ground coordinates after absolute orientation of model epoch 1:

$\Delta\bar{X}$ = 0.20 cm $\Delta\bar{Y}$ = -0.01 cm $\Delta\bar{Z}$ = 0.00 cm

$\sigma_{\Delta X}$ = 22 cm $\sigma_{\Delta Y}$ = 8 cm $\sigma_{\Delta Z}$ = 7 cm

c) subsidence differences between surveying and photogrammetric results:

$\Delta\bar{Z}$ = 10.5 cm , $\sigma_{\Delta Z}$ = 7 cm

The relative accuracy of the system based on c) and the camera-to-object distance was approximately 1/14000 for this approach, while the photo scale was about 1/7000, varying of course significantly, due to the large elevation differences of more than 500 m.

5.3 Cost-Comparison Between Photogrammetric and Ground Surveying Techniques

Once the accuracy requirements of a project are determined, the next step is to find out which design meets these requirements. The choice of the method is based on

i - the availability of suitable equipment (hardware-software)

ii - the appropriate specialized personnel

iii - the project capital-cost

The deciding factor among these three is the last one. For the mapping of large areas, photogrammetric methods are commonly used due to their advantages over ground survey methods, such as lower cost and greater speed. For mining activities topographical mapping is required at several stages of development. During the design stage a map of the general area is often made at 1/5000 or smaller scales, as a base map for geology and for general decisions concerning engineering layouts, e.g., location of spoil piles, access roads and crusher plant sites. Later on, for engineering design, detailed maps at 1/1000 of the mine site are required.

In open-pit and strip mining operations mapping is often carried out on a recurrent basis to provide up-to-date information of the existing situation. These maps are in larger scales, e.g., 1/1000 or 1/2000 and used for the detailed design of pit roads, location of new buildings and dumps and as a graphic representation for reports.

The cost of using aerial photogrammetry over limited areas such as mine sites is often heavily affected by the cost of the photo-

graphy itself. This expense is a function of the remoteness of the mine site from the home base of the flying operation. The photography will most likely cost between $1,000 and $3,000 (CDN) *(Toomey, 1982)*. In addition to this amount, the cost of the photogrammetric equipment must be taken in the account, as well as possible use of computer time.

However, mine management faces high costs in using survey crews for concentrated mapping updates on surface pit operations. For example:

4 days x 3 persons						
1 engineer	x	6 days	x	$400	=	$2,400
2 labourers	x	4 days	x	$150	=	$1,200
						$3,600
Rental of equipment for 4 days						600
		TOTAL				$4,200

In addition, aerial photography will not be used only for measuring displacements but also for mapping of the mining site as has been previously mentioned. Furthermore, in many cases, it offers an alternative measurement of volumes of stockpiles and excavated areas, which so far are measured by ground survey techniques.

Finally, two other important additional applications of aerial photography are the advantages of having a data bank, by forming digital terrain models, and of having a complete record of information.

6

CONCLUSIONS AND RECOMMENDATIONS

The problem of ground subsidence in mining areas is of considerable importance to the densely populated European countries. Only lately have surveyors begun to actively participate in this field in North America due to necessary extensive measurements which could not be tackled by specialists in rock mechanics *(Chrzanowski, 1979)*.

As one of the geometric methods for surface measurements, photogrammetry was tested in the context of this thesis, for monitoring ground subsidence in highly mountainous terrain. The choice of photogrammetric techniques for this purpose was based on the advantages which photogrammetry offers (Chapter 2) with respect to some practical limitations of the other methods previously tested. In this essence, four different approaches were examined, namely: comparison between contour lines, digital elevation model techniques including profiles and regular grid, bundle adjustment methods with self calibration, and direct determination of the object displacements from model coordinate differences. A statistical analysis was performed to evaluate the results, and an economic evaluation of the

system was given.

The comparison of contour lines of an area between two different epochs is an economic analogue method. It offers an overall view of a situation where large displacements have occured. The scale of photography is a deterministic factor in the accuracy of this technique, as well as the quality of the control points used, and the errors introduced during the procedures of the orientations.

The principles of digital elevation models were tested using the analytical plotter AP-2C (O.M.I.). Although these procedures have shown encouraging results in flat areas, difficulties were encountered in inclined terrain. The presence of sliding, combined with vertical movement, led to the measuring of different ground points at each epoch so the results obtained were highly affected by the surface topography.

Therefore, the solution of using discrete points was adopted. Targetted points would be perfect to determine displacements. However, practical conditions did not allow these marked points to be installed. The problem in the identification of the same point in different epochs was circumvented by the suggested 'cross-identification' procedure where the advantages of the stereovision are preserved. The absolute coordinates of the natural points were computed by bundle adjustment programs with self-calibration and the coordinate differences provided the vector of displacements. The accuracy, in this case, was evaluated in the sense of check-point differences. The order of these differences was, on average, 6 cm, while the photo-residuals were of the order of 3.4 μm for x and 9.6 μm for y.

The poor distribution of control points, and consequently the weak geometry of the bundles, resulted in some less accurate areas in the determination of the movements.

The problematic survey and resurvey of the control points, and also of the check points, led to the development of the fourth photogrammetric technique combined again with natural points and presented in this study. Well distributed and surveyed control points are required only during one of the epochs, called epoch zero. The absolute orientation of this model provides the scale and rotations necessary to transform model coordinate differences to the ground displacements. The model coordinate differences are the results of transferring the preceding and subsequent models to model zero. A computer program was written and run on the University's IBM 370/3032 to test this method, and the achieved accuracies were presented in Chapter 5.

As recommendations it should be stressed that:

For any practical applications with a photogrammetric process the random errors must be relatively insignificant compared to the deformations being measured. Thus, the photogrammetric technique must be at least three times, and preferably five to ten times, more accurate than the expected magnitudes of the deformations to be measured *(Kenefick, 1971)*.

Since photogrammetry is a geometric method, an effort must be made to preserve strong geometry during the design and the execution of any photogrammetric project over the area of interest. Furthermore, the specifications set should be kept unchangeable until

the completion of the project.

It is also necessary to evaluate the quality of the obtainable results. An additional field check is always useful to determine the accuracy of the system through statistical tests and to verify the conclusions about the precision of it.

Another important factor to be considered is the stability of the area outside the influence of subsidence. The final results will be affected if the reference points are not fixed as assumed.

In summary, it is recognized *(Chrzanowski et al., 1983)* that subsidence is now a crucial problem in the mining industry. The complexity of monitoring subsidence by classical terrestrial methods makes photogrammetry a useful tool for complete and instantaneous recording of such a dynamic phenomenon over an extended area. Thus the application of photogrammetry can significantly contribute to an integrated monitoring system for subsidence in extreme topographical conditions.

REFERENCES

Allam, M.M. (1976). "The Estimation of Fractures and Slope Stability of Rock Forces using Analytical Photogrammetry", paper presented at the XIII Congress of International Society of Photogrammetry, Helsinki.

American Geological Institute (1962). "Dictionary of Geological Terms", Dolphin Books, Doubleday & Company, Inc., Garden City, New York.

American Society of Photogrammetry (1980). "Manual of Photogrammetry", Published by the American Society of Photogrammetry, 4th edition.

Borchers, E.P. (1968). "Photogrammetric Measurements of Structural Movements", Journal of the Surveying and Mapping Division, January.

Brandenberger, A.J., M.T. Erez (1972). "Photogrammetric Determination of Displacement and Deformations in Large Engineering Structures", The Canadian Surveyor, Vol. 26, No. 2.

Brandow, V.D., H.M. Karara, H.H. Damberger, H.F. Krausse (1976). "A Non-metric Close-Range Photogrammetric System for Mapping Geological Structures in Mines", paper presented at the XIII Congress of International Society of Photogrammetry, Helsinki.

Brown, D.C. (1973). "Accuracies of Analytical Triangulation in Application to Cadastral Surveying", Journal of Surveying and Mapping, American Congress of Surveying and Mapping, Vol. 33, No. 3, September, pp. 281-302.

Brown, D.C. (1981). "LNG Tank Inventory Measurement by Photogrammetry", Proceedings of the American Gas Association, T.127 - T.137.

Chen, Y.Q., A. Chrzanowski (1982). "A General Approach to the Interpretation of Deformation Measurements", Proceedings of the Canadian Institute of Surveying Centennial Convention, Vol. 2, Ottawa, April, 1982, pp. 247-266.

Chrzanowski, A. (1979). "Development Trends in Mining Surveying and Review of Activities of the International Society for Mine Surveying", Proceedings of the 3rd Canadian Symposium on Mining Surveying and Rock Deformation Measurements, Sudbury, Ont., Oct. 10-12.

Chrzanowski, A. W. Faig, B.J. Kurz, A. Makosinski (1980). "Development, Installation and Operation of a Subsidence Monitoring and Telemetry System", Ecological and Resources Consultants Limited, Final Report for Contract No. OSQ78-00238 submitted to CANMET, Calgary, Alberta.

Chrzanowski, A. (1981). "Engineering Surveys - Part I, Collection of Selected Papers and Hand-outs", Department of Surveying Engineering, University of New Brunswick, Fredericton, N.B., Canada.

Chrzanowski, A., W. Faig, (1982a). "Ground Subsidence Determination in Mining Areas", The Indian Mining and Engineering Journal, Vol. XXI, No. 2 and 3.

Chrzanowski, A., W. Faig, M.Y. Fisekci, B. Kurz (1982b). "Telemetric Monitoring of Ground Subsidence over a Hydraulic Mining Operation in the Canadian Rocky Mountains", International Symposium for Mine Surveying, Vol. 3, September 19-25, Varma, Bulgaria.

Chrzanowski, A., B. Kurz (1982c). "A Telemetric System for Monitoring Deformations in Difficult Terrain and Climate Conditions", Proceedings of the 3rd International Symposium on Deformation Measurements by Geodetic Methods, Federation Internationale des Geometres - Commission 6, Vol. 3, Budapest.

Chrzanowski, A., E.F. Hart (1983). "Role of the Surveyor in North America in Studies of Ground Movements in Mining Areas", Presented paper at the American Congress of Surveying and Mapping Annual Convention, Washington, D.C., March.

Dauphin, E., K. Torlegard (1977). "Displacement and Deformation Measurements over Longer Periods of Time", Photogrammetria, 33: pp. 225-239.

Derenyi, E.E. (1972). "The Role of Photogrammetry in Mining and Engineering Surveys", Proceedings of the Canadian Institute of Surveying Annual Meeting, Quebec City.

Earth Satellite Corporation (1975). "Use of Photo Interpretation and Geological Data in the Identification of Surface Damage and Subsidence", Report No. ARC-73-111-2554 prepared for Appalachian Regional Commission, Pennsylvania Department of Environmental Resources.

El-Hakim, S.F. (1982). "The General Bundle Adjustment Triangulation (GEBAT) System - Theory and Applications", Photogrammetric Research, Division of Physics, National Research Council, Ottawa, Canada.

Erlandson, J.P. (1975). "Monitoring Deformations of Structures", Photogrammetric Engineering and Remote Sensing, Vol. 41, No. 11, November, pp. 1375-1384.

Faig, W. (1965). "Photogrammetry Applied to Arctic Glacier Surveys", M.Sc.E. thesis, Department of Surveying Engineering, University of New Brunswick, Fredericton, N.B., Canada.

Faig, W. (1976). "Aerotriangulation", Lecture Notes No. 40, Department of Surveying Engineering, University of New Brunswick, Fredericton, N.B., Canada.

Fenton, P. (1982). "Digital Terrain Modelling Techniques for Volume Calculations and Road Design", Proceedings of the 4th Canadian Symposium on Mining Surveying and Deformation Measurements, June 7-9, Banff, Alberta, pp. 97-114.

Fisekci, M.Y., A. Chrzanowski (1981). "Some Aspects of Subsidence Monitoring in Difficult Terrain and Climate Conditions of Rocky Mountains Western Canada", Proceedings of the Workshop on Surface Subsidence Due to Underground Mining, Nov. 30 - Dec. 2, Morgantown, W.V., pp. 182-196.

Fraser, C.S. (1982). "The Potential of Analytical Close-Range Photogrammetry for Deformation Monitoring", Proceeding of the 4th Canadian Symposium on Mining Surveying and Deformation Measurements, Banff, Alberta, June 7-9, pp. 183-196.

Chosh, S.K. (1972). "Theory of Stereophotogrammetry", Obtainable from the Ohio State University Bookstores, 2nd edition.

Ghosh, S.K. (1975). "Phototriangulation", Lexington Books, D.C. Heath and Company.

Johnson, S., F. Grube (1982). "Photogrammetric Applications in Surface Mining in the United States", International Symposium for Mine Surveying, Vol. 2, Sept. 19-25, Varna, Bulgaria, pp. 225-234.

Johnson, W. (1982). "Monitoring Volcanic Hazards", Bulletin Kern, No. 32, pp. 11-13.

Kenefick, J.F. (1971). "Ultra-Precise Analytical Stereotriangulation for Structural Measurements", paper prepared for presentation at the Symposium on Close-Range Photogrammetry sponsored by the American Society of Photogrammetry, University of Illinois, Urbana, January 26-29.

Kölbl, O., J.J. Stuby (1982). "Mesure de Déplacement du Terrain à l'Aide de Photographies Multi-temporaires", Mensuration Photogrammetrie Genie rural 11/82, Ecole Polytechnique Federale de Lausanne.

Konecny, G. (1963). "Glacial Surveys in Western Canada", presented paper at the 29th Annual Meeting of the American Society of Photogrammetry, Washington, D.C., March.

Masry, S.E. (1977). "Coastal Mapping from a Stereomodel Established using Inertial Platform Data: Errol Analysis", Technical Report No. 49, Department of Surveying Engineering, University of New Brunswick, Fredericton, N.B., Canada.

Masry, S.E., S. MacRitchie (1978). "Can Film Shrinkage be Ignored?", Technical Report No. 51, Department of Surveying Engineering, University of New Brunswick, Fredericton, N.B., Canada.

Mikhail, E.M. (1976). "Observations and Least Squares", Harper & Row, Publishers, Inc., N.Y.

Moffit, F.H., E.M. Mikhail (1980). "Photogrammetry", Harper & Row, Publishers, N.Y., 3rd edition.

Moniwa, H. (1977). "Analytical Photogrammetric System with Self-Calibration and its Applications", Ph.D. Thesis, Department of Surveying Engineering, University of New Brunswick, Fredericton, N.B., Canada.

Morrison, D.F. (1976). "Multivariate Statistical Methods", McGraw-Hill Series, 2nd edition, pp. 164-165.

Norman, J., I. Watson (1975). "Detection of Subsidence Conditions by Photogeology", Engineering Geology, 9: pp. 359-381.

Peterson, J.C. (1976). "Photogrammetric Monitoring of Structural Displacement", Proceedings of the American Society of Photogrammetry Semi-Annual Convention, Seattle.

Richardus, P. (1973). "The Precision of Contourlines and Contour Intervals of Large and Medium Scale Maps", Photogrammetria, Vol. 29, No. 3, pp. 81-107.

Robertson, G.R., A.M.R. Macrae, J. Tribe, D.W. Sibley, D.H. Smith, (1982). "Use of Photogrammetric Methods for Mine Slope Deformation Surveys", Proceedings of the 4th Canadian Symposium on Mining Surveying and Deformation Measurements, Banff, Alberta, June 7-9, pp. 223-231.

Russel, O., R. Ameto, T. Leshendock (1979). "Remote Sensing and Mine Subsidence in Pennsylvania", American Society of Civil Engineers - Transportation Engineering Journal, pp. 185-198.

Saastamoinen, J. (1974). "Local Variation of Photogrammetric Refraction", Photogrammetric Engineering, Vol. XL, No. 3, pp. 295-301.

Somogyi, J. (1982). "Die Rolle der Photogrammetrie im ungorischen Bergbau", Neue Bergbautechnik, 12 Jg, Heft 7, Juli, pp. 380-384.

Sullivan, A. (1978). "Satellite Photos Trace Unstable Mine Roof", Coal Age, September.

Toomey, M.A.G. (1982). "The Application of Digital Terrain Models to Mine Development Mapping", Proceedings of the 4th

Canadian Symposium on Mining Surveying and Deformation Measurements, June 7-9, Banff, Alberta, pp. 89-94.

Vanicek, P., E.J. Krakiwsky (1982). "Geodesy: The Concepts, North-Holland, Amsterdam, Netherlands.

Veress, S.A., L.J. Sunl (1978). "Photogrammetric Monitoring of Gabion Wall", Photogrammetric Engineering and Remote Sensing, Vol. 44, No. 2, February, pp. 205-211.

Veress, S.A., N.C. Jackson, J.N. Hatzopoulos (1980). "Monitoring a Gabion Wall by Inclinometer and Photogrammetry", Photogrammetric Engineering and Remote Sensing, Vol. 46, No. 6, June, pp. 771-778.

Veress, S.A., J.N. Hatzopoulos (1981). "A Combination of Aerial and Terrestrial Photogrammetry for Monitoring", Photogrammetric Engineering and Remote Sensing, Vol. 47, No. 12, pp. 1725-1731.

Veress, S.A., (1982a). "Photogrammetry as a Deformation Survey", Proceedings of the 4th Canadian Symposium on Mining Surveying and Deformation Measurements, Banff, Alberta, June 7-9, pp. 209-221.

Veress, S.A. (1982b). "Deformation Measurements by Aerial and Terrestrial Photogrammetry", III International Symposium on Deformation Measurement by Geodetic Methods, Federation Internationale des Geometres - Commission 6, Budapest, August, Vol. 1.

Wells, D.E., E.J. Krakiwski (1971). "The Method of Least Squares", Lecture Notes No. 18, Department of Surveying Engineering, University of New Brunswick, Fredericton, N.B., Canada.

APPENDIX I

Partial Derivatives

of the

Spatial Similarity Transformation

For a model point whose three ground coordinates are known the elements of the A design matrix defined in eq. (3.17) are:

$$\frac{\partial F_1}{\partial s} = a_{11} = -(r_{11} X_M + r_{21} Y_M + r_{31} Z_M) \quad \text{(I.1)}$$

$$\frac{\partial F_1}{\partial \Omega} = a_{12} = 0 \quad \text{(I.2)}$$

$$\frac{\partial F_1}{\partial \Phi} = a_{13} = s(r_{31} X_M \cos K - r_{31} Y_M \sin K - Z_M \cos \Phi) \quad \text{(I.3)}$$

$$\frac{\partial F_1}{\partial K} = a_{14} = s(r_{11} Y_M - r_{21} X_M) \quad \text{(I.4)}$$

$$\frac{\partial F_1}{\partial X_T} = a_{15} = -1 \quad \text{(I.5)}$$

$$\frac{\partial F_1}{\partial Y_T} = a_{16} = 0 \quad \text{(I.6)}$$

$$\frac{\partial F_1}{\partial Z_T} = a_{17} = 0 \quad \text{(I.7)}$$

$$\frac{\partial F_2}{\partial s} = a_{21} = -(r_{12} X_M + r_{22} Y_M + r_{32} Z_M) \quad \text{(I.8)}$$

$$\frac{\partial F_2}{\partial \Omega} = a_{22} = s(r_{13} X_M + r_{23} Y_M + r_{33} Z_M) \quad \text{(I.9)}$$

$$\frac{\partial F_2}{\partial \Phi} = a_{23} = -\sin \Omega(r_{11} X_M + r_{21} Y_M + r_{31} Z_M) \quad \text{(I.10)}$$

$$\frac{\partial F_2}{\partial K} = a_{24} = s(r_{12} Y_M - r_{22} X_M) \quad \text{(I.11)}$$

$$\frac{\partial F_2}{\partial X_T} = a_{25} = 0 \quad \text{(I.12)}$$

$$\frac{\partial F_2}{\partial Y_T} = a_{26} = -1 \quad \text{(I.13)}$$

$$\frac{\partial F_2}{\partial Z_T} = a_{27} = 0 \tag{I.14}$$

$$\frac{\partial F_3}{\partial s} = a_{31} = - (r_{13} X_M + r_{23} Y_M + r_{33} Z_M) \tag{I.15}$$

$$\frac{\partial F_3}{\partial \Omega} = a_{32} = - s(r_{12} X_M + r_{22} Y_M + r_{32} Z_M) \tag{I.16}$$

$$\frac{\partial F_3}{\partial \Phi} = a_{33} = s \cos \Omega(r_{11} X_M + r_{21} Y_M + r_{31} Z_M) \tag{I.17}$$

$$\frac{\partial F_3}{\partial K} = a_{34} = s(r_{13} Y_M - r_{23} X_M) \tag{I.18}$$

$$\frac{\partial F_3}{\partial X_T} = a_{35} = 0 \tag{I.19}$$

$$\frac{\partial F_3}{\partial Y_T} = a_{36} = 0 \tag{I.20}$$

$$\frac{\partial F_3}{\partial Z_T} = a_{37} = -1 \tag{I.21}$$

The elements of the B design matrix defined in eq. (3.18) are:

$$\frac{\partial F_1}{\partial X_M} = b_{11} = - s r_{11} \tag{I.22}$$

$$\frac{\partial F_1}{\partial Y_M} = b_{12} = - s r_{21} \tag{I.23}$$

$$\frac{\partial F_1}{\partial Z_M} = b_{13} = - s r_{31} \tag{I.24}$$

$$\frac{\partial F_2}{\partial X_M} = b_{21} = - s r_{12} \tag{I.25}$$

$$\frac{\partial F_2}{\partial Y_M} = b_{22} = - s r_{22} \tag{I.26}$$

$$\frac{\partial F_2}{\partial Z_M} = b_{23} = - sr_{32} \tag{I.27}$$

$$\frac{\partial F_3}{\partial X_M} = b_{31} = - sr_{13} \tag{I.28}$$

$$\frac{\partial F_3}{\partial Y_M} = b_{32} = - sr_{23} \tag{I.29}$$

$$\frac{\partial F_3}{\partial Z_M} = b_{33} = - sr_{33} \tag{I.30}$$

The elements of B design matrix, defined in eq. (3.36), with respect to observations corresponding to model epoch 1 and 2 respectively are:

$$\frac{\partial F_1}{\partial X_{M1}} = b_{11} = 1, \frac{\partial F_1}{\partial Y_{M1}} = b_{12} = 0 , \frac{\partial F_1}{\partial Z_{M1}} = b_{13} = 0 \tag{I.31}$$

$$\frac{\partial F_1}{\partial X_{M2}} = b_{14} = - \lambda m_{11}, \frac{\partial F_1}{\partial Y_{M2}} = b_{15} = - \lambda m_{21}, \frac{\partial F_1}{\partial Z_{M2}} = b_{16} = - \lambda m_{31} \tag{I.32}$$

$$\frac{\partial F_2}{\partial X_{M1}} = b_{21} = 0, \frac{\partial F_2}{\partial Y_{M1}} = b_{22} = 1, \frac{\partial F_2}{\partial Z_{M1}} = b_{23} = 0 \tag{I.33}$$

$$\frac{\partial F_2}{\partial X_{M2}} = b_{24} = - \lambda m_{12}, \frac{\partial F_2}{\partial Y_{M2}} = b_{25} = - \lambda m_{22}, \frac{\partial F_2}{\partial Z_{M1}} = b_{26} = - \lambda m_{32} \tag{I.34}$$

$$\frac{\partial F_3}{\partial X_{M1}} = b_{31} = 0, \frac{\partial F_3}{\partial Y_{M1}} = b_{32} = 0, \frac{\partial F_3}{\partial Z_{M1}} = b_{31} = 1 \tag{I.35}$$

$$\frac{\partial F_3}{\partial X_{M2}} = b_{34} = - \lambda m_{13}, \frac{\partial F_3}{\partial Y_{M2}} = b_{35} = - \lambda m_{23}, \frac{\partial F_3}{\partial Z_{M2}} = b_{36} = - \lambda m_{33} \tag{I.36}$$

The elements r_{ij}, m_{ij} of the rotation elements are given in in eq. (3.16), while X_M, Y_M, Z_M and X_{Mi}, Y_{Mi}, Z_{Mi}, i = 1,2 , are model coordinates. The F's functions are given by eq. (3.15).

APPENDIX II

Partial Derivatives

of the

Coplanarity Equation

The evaluation of all partial derivatives is necessary for linearization. The partial derivative of a determinant of order three with respect to a parameter ρ is equal to the sum of three determinants. If R_1, R_2, R_3 are the three rows of a determinant D, then *(Moffit et al., 1980)*

$$\frac{\partial D}{\partial \rho} = \begin{vmatrix} \partial R_1/\partial\rho \\ R_2 \\ R_3 \end{vmatrix} + \begin{vmatrix} R_1 \\ \partial R_2/\partial\rho \\ R_3 \end{vmatrix} + \begin{vmatrix} R_1 \\ R_2 \\ \partial R_3/\partial\rho \end{vmatrix} \qquad \text{(II.1)}$$

The linearized observation equation of eq. (3.55) will have the following form for each pair of conjugate points

$$[a_{11}a_{12}a_{13}a_{14}a_{15}] \begin{bmatrix} \delta B_y \\ \delta B_z \\ \delta\omega''_j \\ \delta\phi''_j \\ \delta\kappa''_j \end{bmatrix} + [b_{11}b_{12}b_{13}b_{14}] \begin{bmatrix} V_{x_i} \\ V_{y_i} \\ V_{x_j} \\ V_{y_j} \end{bmatrix} + \begin{vmatrix} B_x & B_y & B_z \\ u_i & v_i & w_i \\ u_j & v_j & w_j \end{vmatrix} = 0 \qquad \text{(II.2)}$$

The elements a_{ij} and b_{ij} form the design matrices A and B of eq. (3.56). For the first design matrix A they are:

$$\frac{\partial F}{\partial B_y} = a_{11} = \begin{vmatrix} 0 & 1 & 0 \\ u_i & v_i & w_i \\ u_j & v_j & w_j \end{vmatrix} = -\begin{vmatrix} u_i & w_j \\ u_j & w_j \end{vmatrix} = u_j w_i - u_i w_j \qquad \text{(II.3)}$$

$$\frac{\partial F}{\partial B_z} = a_{12} = \begin{vmatrix} 0 & 0 & 1 \\ u_i & v_i & w_i \\ u_j & v_j & w_j \end{vmatrix} = \begin{vmatrix} u_i & v_i \\ u_j & v_j \end{vmatrix} = u_i v_j - u_j v_i \qquad \text{(II.4)}$$

$$\frac{\partial F}{\partial \omega''_j} = a_{13} = \begin{vmatrix} B_x & B_y & B_z \\ u_i & v_i & w_i \\ \frac{\partial u_j}{\partial \omega''_j} & \frac{\partial v_j}{\partial \omega''_j} & \frac{\partial w_j}{\partial \omega''_j} \end{vmatrix} \tag{II.5}$$

$$\frac{\partial F}{\partial \phi''_j} = a_{14} = \begin{vmatrix} B_x & B_y & B_z \\ u_i & v_i & w_i \\ \frac{\partial u_j}{\partial \phi''_j} & \frac{\partial v_j}{\partial \phi''_j} & \frac{\partial w_j}{\partial \phi''_j} \end{vmatrix} \tag{II.6}$$

$$\frac{\partial F}{\partial \kappa''_j} = a_{15} = \begin{vmatrix} B_x & B_y & B_z \\ u_i & v_i & w_i \\ \frac{\partial u_j}{\partial \kappa''_j} & \frac{\partial v_j}{\partial \kappa''_j} & \frac{\partial w_j}{\partial \kappa''_j} \end{vmatrix} \tag{II.7}$$

The partial derivatives in (II.5, 6, 7) are given from

$$\frac{\partial}{\partial \omega''_j} \begin{bmatrix} u_j \\ v_j \\ w_j \end{bmatrix} = \frac{\partial M_j}{\partial \omega''_j} \begin{bmatrix} x_j \\ y_j \\ -f \end{bmatrix} = \left(M_j^T \begin{bmatrix} 0 & 0 & 0 \\ 0 & 0 & 1 \\ 0 & -1 & 0 \end{bmatrix} \right)^T \begin{bmatrix} x_j \\ y_j \\ -f \end{bmatrix} =$$

$$= \begin{bmatrix} 0 & 0 & 0 \\ 0 & 0 & -1 \\ 0 & 1 & 0 \end{bmatrix} \left(M_j \begin{bmatrix} x_j \\ y_j \\ -f \end{bmatrix} \right) = \begin{bmatrix} 0 & 0 & 0 \\ 0 & 0 & -1 \\ 0 & 1 & 0 \end{bmatrix} \begin{bmatrix} u_j \\ v_j \\ w_j \end{bmatrix} =$$

$$= \begin{bmatrix} 0 \\ -w_j \\ v_j \end{bmatrix} \tag{II.8}$$

$$\frac{\partial}{\partial \phi''_j} \begin{bmatrix} u_j \\ v_j \\ w_j \end{bmatrix} = \frac{\partial M_j}{\partial \phi''_j} \begin{bmatrix} x_j \\ y_j \\ -f \end{bmatrix} = \left(M_j^T \begin{bmatrix} 0 & \sin \omega''_j & -\cos \omega''_j \\ -\sin \omega''_j & 0 & 0 \\ \cos \omega''_j & 0 & 0 \end{bmatrix} \right)^T \begin{bmatrix} x_j \\ y_j \\ -f \end{bmatrix} =$$

$$= \begin{bmatrix} 0 & -\sin\omega_j'' & \cos\omega_j'' \\ \sin\omega_j'' & 0 & 0 \\ -\cos\omega_j'' & 0 & 0 \end{bmatrix} \left(M_j \begin{bmatrix} x_j \\ y_i \\ -f \end{bmatrix} \right) = \begin{bmatrix} 0 & -\sin\omega_j'' & \cos\omega_j'' \\ \sin\omega_j'' & 0 & 0 \\ -\cos\omega_j'' & 0 & 0 \end{bmatrix} \begin{bmatrix} u_j \\ v_j \\ w_j \end{bmatrix} =$$

$$= \begin{bmatrix} -v_j \sin\omega_j'' + w_j \cos\omega_j'' \\ u_j \sin\omega_j'' \\ -u_j \cos\omega_j'' \end{bmatrix} \qquad \text{(II.9)}$$

$$\frac{\partial}{\partial\kappa_j''} \begin{bmatrix} u_j \\ v_j \\ w_j \end{bmatrix} = \frac{\partial M_j}{\partial\kappa_j''} \begin{bmatrix} x_j \\ y_j \\ -f \end{bmatrix} = \left(\begin{bmatrix} 0 & 1 & 0 \\ -1 & 0 & 0 \\ 0 & 0 & 0 \end{bmatrix} M_j^T \right)^T \begin{bmatrix} x_j \\ y_j \\ -f \end{bmatrix} =$$

$$= M_j \begin{bmatrix} 0 & -1 & 0 \\ 1 & 0 & 0 \\ 0 & 0 & 0 \end{bmatrix} \begin{bmatrix} x_j \\ y_j \\ -f \end{bmatrix} = M_j \begin{bmatrix} -y_j \\ x_j \\ 0 \end{bmatrix} =$$

$$= \begin{bmatrix} m_{21} x_j - m_{11} y_j \\ m_{22} x_j - m_{12} y_j \\ m_{23} x_j - m_{13} y_j \end{bmatrix} \qquad \text{(II.10)}$$

Substituting (II.8, 9, 10) to (II.5, 6, 7) respectively, the final form of a_{13}, a_{14}, a_{15} is

$$a_{13} = \begin{vmatrix} B_x & B_y & B_z \\ u_i & v_i & w_i \\ 0 & -w_j & v_j \end{vmatrix} \qquad \text{(II.11)}$$

$$a_{14} = \begin{vmatrix} B_x & B_y & B_z \\ u_i & v_i & w_i \\ -v_j \sin\omega_j'' + w_j \cos\omega_j'' & u_j \sin\omega_j'' & -u_j \cos\omega_j'' \end{vmatrix} \qquad \text{(II.12)}$$

$$a_{15} = \begin{vmatrix} B_x & B_y & B_z \\ u_i & v_i & w_i \\ m_{21}x_j - m_{11}y_j & m_{22}x_j - m_{12}y_j & m_{23}x_j - m_{13}y_j \end{vmatrix} \quad \text{(II.13)}$$

The elements of the second design matrix B are:

$$\frac{\partial F}{\partial x_i} = b_{11} = \begin{vmatrix} B_x & B_y & B_z \\ \frac{\partial u_i}{\partial x_i} & \frac{\partial v_i}{\partial x_i} & \frac{\partial w_i}{\partial x_i} \\ u_j & v_j & w_j \end{vmatrix} \quad \text{(II.14)}$$

where

$$\frac{\partial}{\partial x_i}\begin{bmatrix} u_i \\ v_i \\ w_i \end{bmatrix} = M_i \begin{bmatrix} 1 \\ 0 \\ 0 \end{bmatrix} = I \begin{bmatrix} 1 \\ 0 \\ 0 \end{bmatrix} = \begin{bmatrix} 1 \\ 0 \\ 0 \end{bmatrix} \quad \text{(since } M_i = I\text{)} \quad \text{(II.15)}$$

and therefore eq. (II.4) can be written as:

$$b_{11} = \begin{vmatrix} B_x & B_y & B_z \\ 1 & 0 & 0 \\ u_j & v_j & w_j \end{vmatrix} \quad \text{(II.16)}$$

$$\frac{\partial F}{\partial y_i} = b_{12} = \begin{vmatrix} B_x & B_y & B_z \\ \frac{\partial u_i}{\partial y_i} & \frac{\partial v_i}{\partial y_i} & \frac{\partial w_i}{\partial y_i} \\ u_j & v_j & w_j \end{vmatrix} \quad \text{(II.17)}$$

where,

$$\frac{\partial}{\partial y_i}\begin{bmatrix} u_i \\ v_i \\ w_i \end{bmatrix} = M_i \begin{bmatrix} 0 \\ 1 \\ 0 \end{bmatrix} = I \begin{bmatrix} 0 \\ 1 \\ 0 \end{bmatrix} = \begin{bmatrix} 0 \\ 1 \\ 0 \end{bmatrix} \text{(since } M_i = I\text{)} \quad \text{(II.18)}$$

and therefore eq. (II.17) can be written as:

$$b_{12} = \begin{vmatrix} B_x & B_y & B_z \\ 0 & 1 & 0 \\ u_j & v_j & w_j \end{vmatrix} \tag{II.19}$$

$$\frac{\partial F}{\partial x_j} = b_{13} = \begin{vmatrix} B_x & B_y & B_z \\ u_i & v_i & w_i \\ \frac{\partial u_j}{\partial x_j} & \frac{\partial v_j}{\partial x_j} & \frac{\partial w_j}{\partial x_j} \end{vmatrix} \tag{II.20}$$

where,

$$\frac{\partial}{x_j} \begin{bmatrix} u_j \\ v_j \\ w_j \end{bmatrix} = M_j \begin{bmatrix} 1 \\ 0 \\ 0 \end{bmatrix} = \begin{bmatrix} m_{11} \\ m_{12} \\ m_{13} \end{bmatrix}_j \tag{II.21}$$

and therefore eq. (II.20) can be written as

$$b_{13} = \begin{vmatrix} B_x & B_y & B_z \\ u_i & v_i & w_i \\ (m_{11})_j & (m_{12})_j & (m_{13})_j \end{vmatrix} \tag{II.22}$$

$$\frac{\partial F}{\partial y_j} = b_{14} = \begin{vmatrix} B_x & B_y & B_z \\ u_i & v_i & w_i \\ \frac{\partial u_j}{\partial y_j} & \frac{\partial v_j}{\partial y_j} & \frac{\partial w_j}{\partial y_j} \end{vmatrix} \tag{II.23}$$

where,

$$\frac{\partial}{\partial y_j}\begin{bmatrix} u_j \\ v_j \\ w_j \end{bmatrix} = M_j \begin{bmatrix} 0 \\ 1 \\ 0 \end{bmatrix} = \begin{bmatrix} m_{21} \\ m_{22} \\ m_{23} \end{bmatrix}_j \qquad \text{(II.24)}$$

and therefore eq. (II.23) can be written as:

$$b_{14} = \begin{vmatrix} B_x & B_y & B_z \\ u_i & v_i & w_i \\ (m_{21})_j & (m_{22})_j & (m_{23})_j \end{vmatrix} \qquad \text{(II.25)}$$

If elements m_{ij} of the rotation matrix M_j are similar to those defined by eq. (3.16). u_i, v_i, w_i are the refined photo-coordinates of the left photograph and they are equal to x_i, y_i, $-f$ ($M_i = I$), while u_j, v_j, w_j are the refined rotated photo-coordinates of the right photograph and are given by eq. (3.49). The F function is given by eq. (3.54)

APPENDIX III

Atmospheric Refraction

It is well known that density (and hence refractive index) of the atmosphere decreases with increased altitude. As a result, if a ray of light is directed from a point on the ground to the camera lens, such as point P in Figure (III.1), it will be refracted into a curved path away from the vertical at P due to the density gradient of the atmosphere. This refraction is in conformance with Snell's law of refraction. As shown in Fig. (III.1), this refraction causes a small angle $\Delta\Theta$ between the tangent to the actual ray path at the exposure station and the theoretical ray path.

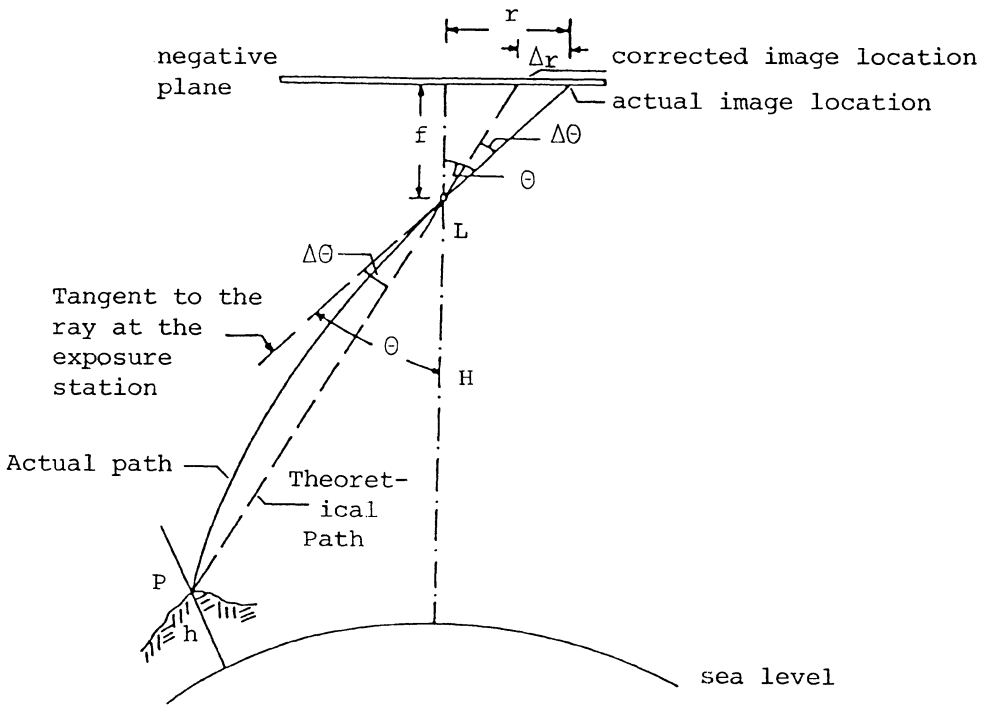

Figure III.1: Atmospheric refraction in vertical aerial photography.

Photogrammetric refraction $\Delta\Theta$ in its simplest form can be expressed as a function of nadir distance Θ *(American Society of*

Photogrammetry, 1980) and is given as

$$\Delta\Theta = R \tan\theta \qquad \text{(III.1)}$$

where R is a function of the vertical density structure of the atmosphere, flying height H and terrain height h. An expression for R is given by Saastamoinen (1974), where he introduces also an expression for the variation of refractive index as a function of height. For flying heights of up to 11 kilometres he gives:

$$R = \frac{2335}{H - h}[(1-0.02257h)^{5.256}-(1-0.02257H)^{5.256}]-277.0(1-0.02257H)^{4.256} \times 10^{-6} \qquad \text{(III.2)}$$

For flying heights over 11 kilometres

$$R = \frac{2335}{H - h}(1-0.02257h)^{5.256}-0.8540^{H-11}\left(82.2+\frac{521}{H-h}\right) \times 10^{-6} \qquad \text{(III.3)}$$

where camera height H and ground height h are both in kilometres above the sea level and R is in μrad.

A formula which expresses the photogrammetric refraction in terms of meteorological element is given by the same author

$$10^{-6}R = 2.316 \left(\frac{p_o - p_H}{H} - 34.11 \, p_H/T_H \right) \qquad \text{(III.4)}$$

where p_o and p_H are the barometric pressures in millibars at the sea level and at the camera level, respectively, H, is the flying height in kilometres above the sea level T_H (= 273.2+ $t_H{}^{o}C$) is the absolute temperature in Kelvin at the camera level and R is in microradians.

Photogrammetric refraction is one of the sources of errors which caused image distortion. The linear distortion on the image plane due to refraction is Δr. Refraction distortion occurs radially from the photographic nadir point (principal point of a vertical photo

and is zero at the nadir point).

From Fig. (III.1) the basic refraction correction equation (for a vertical photograph) may be developed as follows:

From triangle pLp' and the sinus law:

$$\frac{\Delta r}{\sin\Delta\theta} = \frac{Lp}{\sin(90-\theta)} \Rightarrow \Delta r = Lp\,\frac{\sin\Delta\theta}{\cos\theta} \Rightarrow$$

$$\Rightarrow \Delta r = \frac{Lp}{\cos\theta}\Delta\theta \quad (\Delta\theta \text{ in rad}) \tag{III.5}$$

Also

$$Lp = \frac{f}{\cos\theta} \tag{III.6}$$

Substituting eq. (III.6) in eq. (III.5), the latter can be written as

$$\Delta r = \frac{f}{\cos^2\theta}\,\Delta\theta \tag{III.7}$$

Substituting also $\Delta\theta$ from eq. (III.1) into (III.7), Δr is expressed as

$$\Delta r = \frac{f}{\cos^2\theta}\,R\tan\theta = Rr\left(1+\frac{r^2}{f^2}\right) \tag{III.8}$$

After Δr is computed, the corrected image coordinates due to atmospheric refraction can be determined by eq. (3.44). r denotes the radial distance of the photo-point from the principle point of the photograph and is equal to $r = (x_D^2 + y_D^2)^{\frac{1}{2}}$, ($x_D$, y_D are given in eq. (3.43)).

The meteorogical elements affect the photogrammetric refraction. According to Saastamoinen (1974), high barometric pressure, low temperature, strong inverted temperature gradient, and negligible humidity are features which contribute towards strong refraction and, peculiarly, all of them are typical of one extreme of climate and weather. Similarly, the other extreme which

is characterized by low barometric pressure, high temperature, steep negative temperature, and high humidity contains all of the features tending towards weak refraction.

APPENDIX IV

Definitions

Local subsidence: The subsidence phenomena which occur within the mining site and the immediate vicinity.

Regional subsidence: The subsidence phenomena which extend beyond the immediate vicinity of the mining site.

Photogrammetric (or stereoscopic) model: An exact, three-dimensional replica of the ground relief in an arbitrary space and at an arbitrary scale. The stereoscopic model is formed through a process called relative orientation.

Relative orientation: The process (analytical or on a photogrammetric instrument) by which a pair of overlapping photographs are related to one another in some arbitrary space to correspond with their coorientation at the time of photography.

Absolute orientation: The scaling, levelling, and orientation to ground control system of a relatively oriented stereoscopic model or group of models.

Hydraulic method for mining: The method used at the study mine is a roof caving method. The coal seam is normally extracted to a height of 15 m. It lays at a depth from the ground surface of approximately 300-500 m with a dip of 35^{o}. The main roadways and sub-levels (production headings) are driven at about $+7^{o}$ respectively. The distance between the sub-levels is about 25 m and each sub-level is driven to a length of roughly 300 m. The hydraulic jet starts extraction at the upper end of the sub-level and retreats in steps of approximately 15 m. The hydraulic jet also cuts the rise and the gradient of the roadway, providing gravity flow of the coal-water mixture to the dewatering plant.